Photohadronic neutrinos from transients in astrophysical sources

Jörg P. Rachen* and P. Mészáros†
Department of Astronomy and Astrophysics, The Pennsylvania State University, University Park, Pennsylvania 16802
(Received 17 February 1998; published 18 November 1998)

We investigate the spectrum of photohadronically produced neutrinos at very high energies (VHE, $\gtrsim 10^{14}$ eV) in astrophysical sources whose physical properties are constrained by their variability, in particular jets in active galactic nuclei (blazars) and gamma-ray bursts (GRBs). We discuss in detail the various competing cooling processes for energetic protons, as well as the cooling of pions and muons in the hadronic cascade, which impose limits on both the efficiency of neutrino production and the maximum neutrino energy. If the proton acceleration process is of the Fermi type, we can derive a model independent upper limit on the neutrino energy from the observed properties of any cosmic transient, which depends only on the assumed total energy of the transient. For standard energetic constraints, we can rule out major contributions above 10^{19} eV from current models of both blazars and GRBs; and in most models much stronger limits apply in order to produce measurable neutrino fluxes. For GRBs, we show that the cooling of pions and muons in the hadronic cascade imposes the strongest limit on the neutrino energy, leading to cutoff energies of the electron and muon neutrino spectrum at the source differing by about one order of magnitude. We also discuss the relation of maximum cosmic ray energies to maximum neutrino energies and fluxes in GRBs, and find that the production of both the highest energy cosmic rays and observable neutrino fluxes at the same site can only be realized under extreme conditions; a test implication of this joint scenario would be the existence of strong fluxes of GRB correlated muon neutrinos up to ultrahigh energies, $>10^{17}$ eV. Secondary particle cooling also leads to slightly revised estimates for the neutrino fluxes from (nontransient) active galactic nuclei cores, which are commonly used in estimates for VHE detector event rates. Since our approach is quite general we conclude that the detection or nondetection of neutrinos above $\sim 10^{19}$ eV correlated with blazar flares or GRBs (e.g., with the Pierre Auger Observatory) would provide strong evidence against or in favor of current models for cosmic ray acceleration and neutrino production in these sources. [S0556-2821(98)04020-X]

PACS number(s): 95.85.Ry, 98.54.Cm, 98.70.Rz, 98.70.Sa

I. INTRODUCTION

Neutrino astronomy may provide valuable clues for the understanding of the properties of neutrinos and their interactions at energies in the range $10^{14}-10^{19}$ eV, as well as providing qualitatively new information about some of the most interesting cosmic objects. This energy range is also of great interest because it can probe the universe at significantly greater distances than is possible with known stellar sources (e.g., the Sun, or Supernovae such as SN 1987A, produce neutrinos in the ~MeV range through nuclear interactions, which would be difficult to detect from more distant sources due to the overwhelming background of atmospheric neutrinos from cosmic ray air showers [1]). For these reasons, many of the future neutrino telescopes are designed for energies $\gtrsim$TeV, where the atmospheric background becomes negligible. Among the most promising and ubiquitous astrophysical sources of neutrinos at these very high energies are active galactic nuclei (AGN) and gamma-ray bursts (GRB) [2], which have in common that most of their energetic emission appears in short, distinct flares. The study of the physical processes determining the energy spectrum of such neutrino emitting transients is the subject of this paper.

Above TeV energies and up to about 10^{17} eV neutrinos are detected predominantly through the Cherenkov effect in large volumes of water or ice, using the mass of the earth to capture neutrinos and looking for traces of upward going muons from $\nu_\mu \rightarrow \mu$ conversions; above 10^{17} eV air scintillation techniques and large air shower arrays become the most efficient to detect neutrino induced, deeply penetrating horizontal air showers, where electron neutrinos have the advantage to generate showers which are easier to distinguish from the cosmic ray background (see Appendix C for details and references). The major change of detection techniques at about 10^{17} eV motivates the distinction between very high energy (VHE) neutrinos at $10^{14}-10^{17}$ eV and ultrahigh energy (UHE) neutrinos at $\gtrsim 10^{17}$ eV. The most obvious source of UHE neutrinos are interactions of ultrahigh energy cosmic rays with the universal microwave photon background [3], which predict a diffuse neutrino flux strong enough to be detected in air shower experiments [4]. More hypothetical is the prediction of UHE neutrinos from processes associated with grand unification scale physics, e.g., the annihilation topological defects [5]. In the VHE range, the major contribution is expected from AGN [6–11], which are known to emit very high energy gamma rays. A possible contribution of AGN to the UHE neutrino regime is also discussed in connection with the expected event rates of horizontal air showers [12]. Also GRB sources have been proposed as neutrino sources in the MeV–GeV range [13], and at very high energies [14].

Neutrino production in hadronic models of AGN and GRB is generally attributed to the acceleration of protons in shocks or plasma turbulence, known as Fermi acceleration.

*Email address: jrachen@astro.psu.edu
†Email address: pmeszaros@astro.psu.edu

These energetic protons then interact with soft background photons to produce pions (photohadronic pion production). VHE-UHE neutrinos originate in the decay of charged pions, boosted in energy by the original proton Lorentz factor, and maybe by an additional Doppler factor due to the bulk motion of the rest frame of the relativistic outflows or jets which characterize these sources. The associated decay of neutral pions leads to the production of gamma rays, and it has been claimed that the observed emission up to $\gtrsim$10 TeV in Doppler boosted AGN jets [15] is due to this process rather than inverse Compton scattering of photons by energetic electrons [16]. A relevant issue is that there are alternative models of AGN and GRB where the momentum and energy flux of the relativistic jets or outflows are provided by $e^{\pm}$ or magnetic fields (e.g., [17,18] and references therein), rather than protons, and these would be expected to have negligible neutrino fluxes. The positive identification of VHE-UHE neutrinos from AGN and GRB would be an indication for baryon loaded outflows. The energetic protons may also contribute to the highest energy cosmic ray spectrum, which is observed up to 3×10^{20} eV [19], where AGN and GRBs are considered among the most plausible sources. Here also, the observation or nonobservation of energetic neutrinos would be a crucial test for these models.

The details of the photohadronic production of neutrinos via pion decay depend strongly on the properties of the source, i.e., its size, lifetime, magnetic field, etc. The magnitude of these quantities are estimated from the observed variability, flux, and the measured or inferred distance of these sources. GRB usually last 0.1–100 s, but show intrinsic variability down to milliseconds, while AGN emit most of their energetic radiation in strong flares lasting several weeks, with intrinsic variability on time scales of days down to less than one hour. The transience of energetic emission could improve the association of detected neutrinos with their putative sources, because one could use both arrival direction and arrival time information, allowing statistically significant statements even for total fluxes below the background level.

On the other hand, transience and variability sets constraints on the maximum energy of the neutrino spectrum. In the literature so far, this has been connected to the maximum proton energy using simple kinematical relations. As we show in this paper, however, in these astrophysical scenarios the secondary particles in the photohadronic cascade, i.e., pions and muons, have to be considered separately, since cooling processes can have a significant impact on their final distribution. Moreover, one needs to evaluate carefully the competing proton energy loss processes that do not lead to neutrinos, which can cause breaks in the neutrino spectrum that are not present in the proton spectrum, and thus strongly limit the predicted fluxes at very high energies.

Starting with a general treatment of photohadronic neutrino production in variable sources, we derive a general upper limit for the maximum energy of neutrinos produced by photohadronic interactions of Fermi accelerated protons in cosmic transients, which only depends on the total energy of the transient and observational parameters, like duration or (photon) luminosity. We then apply our results to hadronic AGN and GRB models, and find that they impose severe constraints on their possible contribution to the UHE neutrino spectrum. Notational conventions used throughout the paper and frequently used symbols are explained in Appendix A.

II. PHOTOHADRONIC NEUTRINO PRODUCTION

A. Proton cooling and neutrino production efficiency

Photohadronic neutrino production is a result of the decay of charged pions originating from interactions of high energy protons with ambient low energy photons. It is accompanied by the production of gamma rays from neutral pion decay; the details of the process are described in Appendix B, for a target photon spectrum following a power law with index a above a break energy ϵ_b. For the proton gas, pion production acts as a cooling process, and is in competition with other cooling processes like Bethe-Heitler pair production, synchrotron radiation, cosmic ray emission, and adiabatic losses due to the expansion of the emission region.

While neutrinos are exclusively produced by charged pion decay, gamma rays are produced by a variety of processes: besides neutral pion decay, $\pi^0\rightarrow\gamma\gamma$, the major hadronically induced channels are synchrotron radiation from (a) the UHE protons themselves, (b) the electrons, muons, and charged pions in the photohadronic decay chain (see Appendix B), and (c) the Bethe-Heitler pairs produced in $p\gamma\rightarrow pe^+e^-$ interactions [20]. If synchrotron cooling of secondary particles is negligible, about 25% of the energy in charged pions is converted into gamma radiation by synchrotron cooling of the electron produced in muon decay [16,21]. Normally, the first generation gamma rays cannot leave the emission region, but rather induce an electromagnetic cascade through pair production with low energy background photons, and subsequent synchrotron radiation of electrons and positrons. They cascade down in energy, until they eventually escape below some critical energy where the emission region becomes optically thin [21]. Hadronically induced gamma rays are usually in competition with synchrotron and inverse Compton photons radiated by primary energetic electrons.

Cosmic rays can be ejected in essentially two ways: (a) if the emission region has a sharp boundary beyond which the magnetic field drops rapidly, protons scattered across the boundary would be ejected, and (b) secondary neutrons produced in $p\gamma$ interactions can escape if (b1) their decay length in the comoving frame is larger than the size of the emission region, $c\tau_n\gg R$ with $\tau_n=\gamma_p\tau_n^{\rm RF}$, and (b2) their probability of reconversion to a proton by, e.g., a reaction $n\gamma\rightarrow p\pi^-$ is small, expressible by $ct_{n\rightarrow p}\gg R$. Process (a) depends on the detailed structure of the emission region and is usually in competition with adiabatic cooling, which affects charged particles due to the adiabatic invariance of the quantity $Br_{\rm L}^2$ during the Larmor motion of the particle ($r_L=E/eB$ is the Larmor radius) in a magnetic field decreasing with expansion [22]. In an isotropically expanding emitter with conserved total magnetic energy this means $B\propto R^{-2}$, and thus $E\propto R^{-1}$, but other dependences may apply (see Sec. III B1). Process (b) is tightly connected to neutrino production, because the dominant channel producing charged pions,

$p\gamma \to n\pi^+$, is also the dominant channel for neutron production. The time scale for proton-neutron conversion is $t_{p\to n} \approx t_{n\to p} \approx 2t_{p,\pi}$, which is larger than the time scale for charged pion production, $t_{\pi^\pm} \approx \frac{3}{2} t_{p,\pi}$ (Appendix B), because there the process $p\gamma \to p\pi^+\pi^-$ contributes considerably.

The efficiency of neutrino production depends on (i) which fraction of their energy protons convert into charged pions, and (ii) the fraction of energy pions and muons retain until they decay. Condition (ii) can be quantified by introducing the efficiency of energy conversion from the originally produced pion into neutrinos, $\zeta^{\rm dc}_{\nu,\mu} = \frac{1}{2}(\gamma^{\rm dc}_\mu/\gamma^{\rm pr}_\pi)$ and $\zeta^{\rm dc}_{\nu,\pi} = \frac{1}{4}(\gamma^{\rm dc}_\pi/\gamma^{\rm pr}_\pi)$, for muon and pion decay, respectively, where $\gamma^{\rm pr}_\pi \approx \gamma_p$ is the Lorentz factor of the pion at production, and $\gamma^{\rm dc}_\mu \leqslant \gamma^{\rm dc}_\pi \leqslant \gamma^{\rm pr}_\pi$ are the Lorentz factors of the muon and the pion, respectively, at their decay (see Appendix B and Sec. III C). Similarly we can quantify (i) by introducing the charged pion production efficiency, $\zeta_{\pi^\pm} = t_p/t_{\pi^\pm}$, where t_p is the total cooling time of the proton. This leads to the total neutrino production efficiency

$$\zeta_\nu(\gamma_p) = \zeta_{\pi^\pm}(\zeta^{\rm dc}_{\nu,\pi} + \zeta^{\rm dc}_{\nu,\mu}) \approx \left(\frac{1}{3}\frac{\gamma^{\rm dc}_\mu}{\gamma_p} + \frac{1}{6}\frac{\gamma^{\rm dc}_\pi}{\gamma_p}\right)\frac{\overline{t_p}}{t_{p,\pi}}. \quad (1)$$

The total proton cooling time is determined by the inverse sum, $\overline{t_p}^{-1} = \Sigma_i t^{-1}_{p,i}$, extending over all participating cooling processes. To classify the cooling processes by their dependence on γ_p, we introduce total cooling times for photohadronic interactions, $t_{p\gamma}$, synchrotron radiation, $t_{p,\rm syn}$, and external cooling processes, $t_{\rm ec}$. Under external cooling processes we subsume adiabatic cooling, which has a time scale $t_{\rm ad}$ independent of the proton energy, and direct ejection of protons from the emission region. The latter may be dependent on the proton energy if diffusive losses are relevant; in the simplest case, however, we can assume that protons are confined over the time scale set by adiabatic expansion, i.e., $t_{{\rm esc},p} \geqslant t_{\rm ad}$, which means that

$$t_{\rm ec} \approx t_{\rm ad} = {\rm const}(\gamma_p). \quad (2)$$

The synchrotron loss time can be written as

$$t_{p,\rm syn} = t_{\rm b,syn}\left(\frac{\gamma_p}{\gamma_{\rm b}}\right)^{-1} \quad \text{with} \quad t_{\rm b,syn} = \frac{9c}{4r_p\omega^2_{B,p}\gamma_{\rm b}}, \quad (3)$$

where $r_p = e^2/m_pc^2 \approx 1.5\times 10^{-16}$ cm is the classical proton radius, and $\omega_{B,p} = eB/m_pc$ is the cyclotron frequency of the proton. The characteristic proton Lorentz factor used here for normalization,

$$\gamma_{\rm b} \equiv \epsilon^{\rm RF}_{\rm th}/2\epsilon_{\rm b} \quad (4)$$

expresses the limit above which all photons in the power law part of the spectrum are boosted above the reaction threshold for pion production, assuming that the photon number spectrum can be described as a power law, $dN_{\rm ph} \propto \epsilon^{-a} d\epsilon$, with an index $a > 1$ above some break energy $\epsilon_{\rm b}$ (see Appendix B for details). The cooling time for pion production can then be written in a similar way as

$$t_{p,\pi} = t_{{\rm b},\pi}(\gamma_p/\gamma_{\rm b})^{1-a} \quad \text{for} \quad \gamma_p < \gamma_{\rm b}, \quad (5a)$$

$$t_{p,\pi} \approx t_{{\rm b},\pi}(N_{\rm ph,b}/N_{\rm ph}) \quad \text{for} \quad \gamma_p \gg \gamma_{\rm b}, \quad (5b)$$

where $N_{\rm ph}$ is the total photon density, $N_{\rm ph,b}$ is the density of photons with $\epsilon > \epsilon_{\rm b}$. $t_{{\rm b},\pi}$ is the pion production cooling time for protons with $\gamma_p = \gamma_{\rm b}$, and can be expressed as $t_{{\rm b},\pi} = [cN_{\rm ph,b}{\rm H}_a]^{-1}$, where $\rm H_a$ is the inelasticity weighted effective cross section for pion production, as defined in Appendix B.

The time scales for other photohadronic cooling processes, including neutron ejection, can all be expressed in $t_{p,\pi}$. The cooling time for the Bethe-Heitler process can be evaluated similarly to Eqs. (5a), (5b) and (B2); the inelasticity weighted cross section for the Bethe-Heitler process is ${\rm H}_{a,\rm BH} \approx {\rm H}_a/125$, for a break Lorentz factor $\gamma_{\rm b,BH} \approx \gamma_{\rm b}/140$, leading to $f_{\rm BH} \equiv t_{p,\pi}/t_{p,\rm BH} \approx \exp(5a-10)$ for $\gamma_p \lesssim \gamma_{\rm b,BH}$, and $f_{\rm BH} \ll 1$ for $\gamma_p \gg \gamma_{\rm b,BH}$. To quantify the time scale for energy loss due to free neutron escape, $t_{{\rm esc},n}$, we introduce the probabilities for neutron-to-proton reconversion within the length scale of the emission region R, due to beta decay, $P_{n\beta} = \exp(-c\tau_n/R)$, and due to pion production, $P_{n\gamma\to p} \approx \exp(-2ct_{p,\pi}/R)$, using $t_{n\to p} \approx 2t_{p,\pi}$. Since the typical energy ratio of the neutron to the pion in a $p\gamma \to n\pi^+$ reaction is ≈ 4, we finally get $t_{{\rm esc},n} \approx \frac{1}{2}P^{-1}_{{\rm esc},n}t_{p,\pi}$, where $P_{{\rm esc},n} = (1 - P_{n\gamma\to p})(1 - P_{n\beta})$ is the probability of the neutron to escape. With $t^{-1}_{p\gamma} \equiv t^{-1}_{p,\pi} + t^{-1}_{{\rm esc},n} + t^{-1}_{p,\rm BH}$, and using the fact that beta decay and photohadronic interactions for neutrons are likely in different Lorentz factor regimes, viz., $P_{n\beta}P_{n\gamma\to p} \ll 1$, we can write

$$f_{p\gamma} \equiv \frac{t_{p,\pi}}{t_{p\gamma}} \approx 3 + \exp(5a-10) - 2\exp\left(-\frac{c\tau^{\rm RF}_n\gamma_p}{R}\right) - 2\exp\left(-\frac{2ct_{p,\pi}}{R}\right) \quad (6)$$

for $\gamma_p \lesssim 0.01\gamma_{\rm b}$. For $\gamma_p \gtrsim \gamma_{\rm b}$, the term expressing the Bethe-Heitler efficiency, $\exp(5a-10)$, is absent. Assuming $t_{\rm ec} \approx t_{\rm ad}$ we can write

$$\frac{t_{p,\pi}}{\overline{t_p}} = (t^{-1}_{p\gamma} + t^{-1}_{p,\rm syn} + t^{-1}_{\rm ec})t_{p,\pi} \approx \max(f_{\rm ad}, f_{p\gamma}, f_{\rm syn}) \equiv f_{\rm max}, \quad (7)$$

where $f_{\rm syn} \equiv t_{p,\pi}/t_{p,\rm syn}$ and $f_{\rm ad} \equiv t_{p,\pi}/t_{\rm ad}$ are defined analogously to $f_{p\gamma}$, i.e., expressing the energy dissipated in the various cooling channels in units of the energy lost in pion production. The approximation by the maximum-function is best if one cooling process clearly dominates, and is useful for the following, qualitative discussion of the spectral distribution of emitted neutrinos.

B. Shape of the time integrated neutrino spectrum

Because of the low detection efficiency of neutrinos at earth, it is impossible with present techniques to observe short scale time variability of cosmic neutrino spectra. Therefore, for an outburst active over a limited time, it is more meaningful to calculate the time integrated neutrino

count spectrum, rather than the spectral count rate at a fixed time. This also simplifies the theoretical treatment, because we do not need to perform a self consistent calculation of the accumulated proton spectrum at a specific time—the energy input at any specific energy is simply given by the time integrated proton injection spectrum.

Clearly, the proton spectrum injected by the acceleration process is not directly observable. We will follow here the scenario assumed in most models, that the average injection rate for energetic protons follows a power law in energy, $\langle d\dot{N}_p\rangle = I_p \gamma_p^{-s} d\gamma_p$, extending from some minimum Lorentz factor $\check{\gamma}_p$ to a maximum Lorentz factor $\hat{\gamma}_p \gg \check{\gamma}_p$. We assume that the injection is active over a time $T_{\rm inj}$, and that the injection spectrum does not change in time. Then the total, time integrated energy density of injected protons is given by

$$\overline{u_p} = T_{\rm inj} \int_{\check{\gamma}_p}^{\hat{\gamma}_p} m_p c^2 \gamma_p \langle d\dot{N}_p\rangle_{\gamma_p} = b_p m_p c^2 T_{\rm inj}\, I_p \hat{\gamma}_p^{2-s}, \quad (8)$$

where b_p is the bolometric correction factor of the proton spectrum relative to its energy content at the highest particle energies, given as $b_p = |(\hat{\gamma}_p/\check{\gamma}_p)^{s-2} - 1|/|s-2|$ for $s \neq 2$ and $b_p = \ln(\hat{\gamma}_p/\check{\gamma}_p)$ for $s = 2$.

Protons injected at a specific Lorentz factor γ_p produce charged pions with $\gamma_\pi^{\rm pr} \approx \gamma_p$ at a rate $t_{\pi^\pm}^{-1}$, over a time $\overline{t_p}$. Thus, the total number density of charged pions produced in the emission process is $dN_\pi = \frac{2}{3} T_{\rm inj} \langle d\dot{N}_p\rangle \overline{t_p} t_{p,\pi}^{-1}$. Each charged pion produces two muon neutrinos ($\nu_\mu \bar{\nu}_\mu$) and one electron neutrino (ν_e or $\bar{\nu}_e$), each with an energy $E_\nu \approx \frac{1}{4} m_\pi c^2 \gamma_p$ if we assume that $\gamma_\mu^{\rm dc} \approx \gamma_\pi^{\rm dc} \approx \gamma_p$. Then, the total time integrated neutrino power at the energy E_ν emitted by the source in its rest frame is

$$\overline{L_\nu}(E_\nu) \equiv E_\nu \frac{dN_\nu}{d\,\ln E_\nu} = \frac{m_\pi}{m_p} \frac{V\overline{u_p}}{b_p \hat{\gamma}_p^{2-s}} \Phi\left(\frac{4E_\nu}{m_\pi c^2}\right), \quad (9)$$

where V is the volume of the emission region. The spectral shape is expressed by the function $\Phi(\gamma_p) = \gamma_p^{2-s} \zeta_\nu(\gamma_p)$, which can be written as $\Phi(\gamma_p) = \gamma_p^{2-s} f_{\rm max}^{-1}(\gamma_p) \propto \gamma_p^q$ in the case of one dominating cooling process; the power law index q is, depending on the dominant cooling process, given by

$\Phi(\gamma_p) \propto \gamma_p^q$:	$\gamma_p \lesssim \gamma_{\rm b}$	$\gamma_p \gg \gamma_{\rm b}$
$f_{\rm max} = f_{\rm ad}$:	$q = a - s + 1$	$q = 2 - s$
$f_{\rm max} = f_{p\gamma}$:	$q = 2 - s$	$q = 2 - s$
$f_{\rm max} = f_{\rm syn}$:	$q = a - s$	$q = 1 - s$,

(9a)

where a is the target photon spectral index. For $a > 2$, an additional spectral modification will occur due to the drop of the Bethe-Heitler efficiency between $\sim 0.01\gamma_{\rm b}$ and $\sim \gamma_{\rm b}$, if photohadronic cooling is dominant in this region ($f_{\rm max} = f_{p\gamma}$); in this case, one would expect a rapid rise in the neutrino flux in the regime $E_\nu \lesssim (30\ {\rm MeV})\gamma_{\rm b}$.

The energy dependence of neutrino event rate as observed in a given detector follows closely the neutrino power spectrum, as shown in Appendix C, if we properly account for energy shifts due to Doppler boosting or source redshift, i.e., we expect an increase of events with energy for $q > 0$, a decrease for $q < 0$, and $q \approx 0$ would indicate an event rate almost independent of energy. The dominant proton cooling process in the source, and thus the value of q may change with energy. Obviously, such a transition of cooling processes at some energy, leading to a spectral break, can only occur if the process taking over has a cooling time decreasing faster with energy. Therefore, the spectrum steepens at each break, and for $\hat{\gamma}_p < \gamma_{\rm b}$ the only possible sequence of break energies is $\tilde{E}_{p\gamma} \leqslant \tilde{E}_{{\rm syn}(p)} \leqslant \hat{E}_p$ for $a < 2$, and $\tilde{E}_{{\rm syn}(p)} \leqslant \tilde{E}_{p\gamma} \leqslant \hat{E}_p$ for $a > 2$, while only one break can exist for $a = 2$ or above $\gamma_{\rm b}$ [cf. Eq. (9a)]. However, depending on the source properties it may be that some cooling processes are never dominant, so not all possible break energies may appear in the spectrum [cf. Sec. IV A and Fig. 1 for an example]. If the proton spectral index is close to the canonical value for shock acceleration, $s \approx 2$, we would generally expect an increasing event rate at low energies in the regime of adiabatic cooling dominance, and a flat behavior ($q \approx 0$) if photohadronic cooling becomes dominant, which can be most easily understood as a saturation of the efficiency, Eq. (1). The efficiency can decrease again if proton synchrotron cooling becomes dominant (for $a < 2$), unless the proton spectrum cuts off first. The possible cooling of secondary particles in the hadronic cascade may lead to additional breaks, as discussed in Sec. III C 2, and illustrated in an example in Sec. IV B and Fig. 2.

III. NEUTRINO EMISSION FROM COSMIC TRANSIENTS: GENERAL THEORY

Although neutrino bursts themselves may only be observable in their time integrated appearance, the accompanying burst of photons is observable in much greater detail, and allows to constrain the physical parameters determining neutrino production. We have to distinguish between low energy photons, which are in general explained by synchrotron radiation of electrons coaccelerated with the protons, and high energy gamma radiation which may be dominated by hadronically induced cascades, as discussed above, but could also originate dominantly from inverse Compton photons produced by the electrons. The terms ''low energy'' and ''high energy'' are here used only in a relative meaning—the absolute energy range for electron synchrotron radiation on the one hand, and electron Compton radiation or hadronically induced photons on the other, depends strongly on the physical conditions at the source. The following discussion is more focussed on the low energy photon component, which is relevant as the target population for photohadronic neutrino production. However, if the high energy photons are of hadronic origin, their variability can also give valuable clues on proton cooling times.

Hereafter we distinguish between physical quantities defined in the comoving frame of the source and observed quantities (see Appendix A for notational conventions), where we account for a possible boosting of the radiation emitted from the source with a Doppler factor $\mathcal{D} = [\Gamma(1 - \beta_\Gamma \cos\Theta_{\rm view})]^{-1}$ for a relativistic flow with Lorentz factor Γ and a velocity $\beta_\Gamma c$ under an angle $\Theta_{\rm view}$ to the

direction of the observer. We do not take into account cosmological redshift effects, and just note that they might be considered by replacing $\mathcal{D}=\mathcal{D}'/(1+z)$, if $\mathcal{D}'$ is the Doppler factor of the emission region in the cosmologically comoving frame at the source. The task of this section is to constrain the physical properties of the emission region by observable quantities, in order to discuss the various processes limiting the neutrino energy.

A. Variability time scales and the size of the emission region

1. The causality limit

If a flare occurring in a relativistic outflow, boosted with a Doppler factor $\mathcal{D}$, is observed to have a duration $\mathcal{T}$, the time scale of the burst in the comoving frame of the fluid is $T=\mathcal{T}\mathcal{D}$. This flare time scale covers (a) the time scale for the injection of energetic particles, $T_{\rm inj}$, (b) the time scale over which the particles convert their energy in radiation, $T_{\rm rad}$, and (c) the crossing time the photons need to leave the emission region in the direction of the observer, $T_{\rm cr}$. The partial times normally do not simply add up, but by order of magnitude the estimate

$$T\sim\max(T_{\rm inj},T_{\rm rad},T_{\rm cr}) \tag{10}$$

applies. The crossing time is naturally connected to the (comoving) linear size of the emission region; if the emission region is not spherically symmetric, we can only limit the comoving size along the line of sight, $R_{\parallel}$, by the observed duration as

$$R_{\parallel}=cT_{\rm cr}=c\rho_T\mathcal{T}\mathcal{D}, \tag{11}$$

where the factor $\rho_T\leqslant 1$ considers the effect of a delayed emission due to finite injection or radiation time scales; $\rho_T=1$ means that the emission is homogeneous and instantaneous within the size R—the observed duration is then simply the time between the first and the last photon reaching us. Since the condition $T\geqslant T_{\rm cr}$ is equivalent to the requirement that the emission throughout the emission region is due to one, causally connected process, Eq. (11) may be called the *causality limit* for the size of the transient source. The projected (or lateral) comoving size, $R_{\perp}$, is not constrained by the variability time scale, but plays a role for the determination of the internal radiation density of the emission region from its observed, isotropized luminosity at a specific photon energy, $\mathcal{L}(\varepsilon)=4\pi d_L^2\varepsilon^2(dN_{\rm ph}/d\varepsilon)_{\rm obs}=\mathcal{D}^4L(\epsilon)$ with $\varepsilon=\mathcal{D}\epsilon$, where d_L is the luminosity distance of the source (note that the redshift is absorbed in the Doppler factor, as explained above). To account for this, we introduce a geometrical eccentricity parameter, x_L, by writing the luminosity as

$$L(\epsilon)=4\pi R_{\parallel}^2cx_L\epsilon^2(dN_{\rm ph}/d\epsilon), \tag{12}$$

where $\epsilon^2(dN_{\rm ph}/d\epsilon)$ is the specific energy density of photons with energy ϵ in the rest frame of the flow. For a spherically symmetric emission region $x_L=1$, while a disklike emission region ($R_{\parallel}\ll R_{\perp}$) would be described by $x_L\sim(R_{\perp}/R_{\parallel})^2\gg 1$.

The radiation time scale is obviously equivalent to the cooling time scale of the radiating particles; for radiation processes involving electrons, it is usually very short, $T_{\rm rad}\ll T_{\rm cr}$, justifying its neglect. If we consider radiation produced in photohadronic interactions, we can write $T_{\rm rad}\approx\overline{t_p}$, since the time scale over which the electromagnetic cascade evolves can be considered as short compared to $\overline{t_p}$. $T_{\rm inj}$ is the time over which an acceleration process is active, e.g., the lifetime of a shock. Obviously, this sets a limit on the acceleration time of the particles, $t_{\rm acc}<T_{\rm inj}<\mathcal{T}\mathcal{D}$. Also here, this is barely relevant for electrons, but sets an important limit for protons.

2. The internal shock scenario

As an example how observed time scales in transient emission phenomena may be connected to the size of the emission region, we discuss the scenario of energy conversion in relativistic flows by internal shocks. This scenario was suggested originally by Rees [23] for AGN jets, and was later also applied to gamma-ray bursts [24].

We consider two plasma blobs of similar mass and density emitted within an unsteady flow at times t_1 and t_2, $\Delta t=t_2-t_1>0$, with respective Lorentz factors Γ_1 and Γ_2, $\Gamma_2/\Gamma_1\gtrsim 1$, i.e., the second blob has a larger velocity and thus catches up with the first after some time $\sim\Gamma_1\Gamma_2\Delta t$. Assuming that their relative velocities are supersonic, two strong shock waves moving in opposite directions form when the blobs merge; they are called *forward shock* and *reverse shock*, respective to their direction of motion relative to the flow. In their center of mass frame (CMF), which has a Lorentz factor $\Gamma\approx\sqrt{\Gamma_1\Gamma_2}$ in the observers frame, the shocked material in region between the two shocks is at rest, and is the source of the radiation. The shocks move each with a velocity $\beta_{\rm sh}c$, $\beta_{\rm sh}\approx\sqrt{1-\Gamma_1/\Gamma_2}$, corresponding to an internal shock Lorentz factor $\Gamma_{\rm sh}\approx\sqrt{\Gamma_2/\Gamma_1}$. The linear size of the emitter in the direction of the flow, after the merging is complete, is $R_{\parallel}=2R'_{\parallel}/\chi_\rho$, if $R'_{\parallel}$ is the length of the blobs in this direction in their respective rest frames, and $\chi_\rho=4\Delta\Gamma+3$ is the compression factor [25]. Therefore, $T_{\rm inj}\approx R'_{\parallel}/c\chi_\rho\beta_{\rm sh}=T_{\rm cr}/2\beta_{\rm sh}$, which is the time each shock needs to cross half this distance. For transrelativistic internal shocks, $\beta_{\rm sh}\approx\frac{1}{2}$, the crossing time is therefore a good measure for the injection time scale. The total efficiency for the dissipation of energy by the shocks is given by $\xi_{\rm sh}=1-2\Gamma_{\rm sh}/(1+\Gamma_{\rm sh}^2)$, and is about 20% for $\Gamma_{\rm sh}\approx 2$.

We now assume that the radiation time scale is much shorter than the dynamic time scales involved in the shock merging. Then, the emission follows closely the motion of the shocks; if the observer is placed at an angle $\Theta_{\rm view}\ll 1$ to the flow direction, the emission of the forward shock appears as a peak of duration $\mathcal{T}_{\rm f}=T_{\rm inj}\mathcal{D}^{-1}(1-\beta_{\rm sh})$ in the observer frame, while the emission of the reverse shock causes a peak with a duration $\mathcal{T}_{\rm r}=T_{\rm inj}\mathcal{D}^{-1}(1+\beta_{\rm sh})$ and comparable total energy. For $\beta_{\rm sh}\approx 1/2$, the two peaks can thus have different lengths (but of the same order of magnitude), and the total, superposed peak might appear asymmetric, with a rise time $\mathcal{T}_{\uparrow}\approx\mathcal{T}_{\rm f}/2\mathcal{D}$, and a decay time $\mathcal{T}_{\downarrow}\approx(\mathcal{T}_{\rm r}-\frac{1}{2}\mathcal{T}_{\rm f})/\mathcal{D}$. The crossing

time is then correctly estimated by $T_{\rm cr}=\mathcal{T}\mathcal{D}$ (or $\rho_T=1$), if we define

$$\mathcal{T}\equiv\mathcal{T}_{\rm r}-\mathcal{T}_{\rm f}\approx\mathcal{T}_{\downarrow}-\mathcal{T}_{\uparrow}. \tag{13}$$

We stress that this result is independent of $\beta_{\rm sh}$. Equation (13) makes use of two assumptions: (a) that the two plasma blobs have comparable densities, and (b) that $T_{\rm rad}\ll T_{\rm cr}$. Condition (b) is mostly satisfied, if we consider synchrotron of inverse radiation from energetic electrons. Condition (a) can be assumed to nearly satisfied in internal shocks—which is the most important difference to *external* shocks, where the densities are usually very different. If (a) is not satisfied, forward and reverse shock have different velocities in the CMF, and also different efficiencies in energy conversion [25,26]: hence, the forward and backward peak have very different strengths, and the correlation of $\mathcal{T}_{\rm f}$ and $\mathcal{T}_{\rm r}$ with $\mathcal{T}_{\uparrow}$ and $\mathcal{T}_{\downarrow}$ is less straightforward. If (b) is not satisfied, i.e., if $T_{\rm rad}>T_{\rm cr}$, we expect $T_{\rm rad}\sim\mathcal{T}_{\downarrow}\mathcal{D}$, and $T_{\rm cr}\sim\mathcal{T}_{\uparrow}\mathcal{D}$. A similar situation arises for fast cooling, but the presence of a secondary acceleration process which is not associated to the shock waves (e.g., second order Fermi acceleration; see Appendix D), which can keep up a population of energetic particles homogeneously over the region of the shocked gas, and thus extend the emission as in the case of slow cooling. Despite these ambiguities, we may assume that for flares with considerable asymmetry, $\mathcal{T}_{\downarrow}-\mathcal{T}_{\uparrow}>\mathcal{T}_{\uparrow}$, Eq. (13) gives a reliable upper limit on the crossing time. We also note that the geometrical eccentricity parameter, x_L, as introduced in Eq. (12), satisfies the relation $x_L=\chi_\rho^2 x_L'$, if x_L' is the eccentricity of the blobs before they merge. Since $\chi_\rho^2\gtrsim 10$ for transrelativistic shocks, this may give rise to assume rather disklike geometries in the internal shock scenario; this conclusion, however, may not be overinterpreted because we can obviously not rule out that the blobs have been originally elongated in the flow direction, i.e., $x_L'<1$. The internal shock mechanism can readily be applied to spherical (or quasispherical) outbursts, where the up-catching ''blobs'' have to be replaced by shells emitted with different velocities at different times [24]. We discuss this scenario, and its implication for the geometrical factors ρ_T and x_L, in more detail in Sec. IV B1.

B. Maximum energy of accelerated protons

The predominance of power laws in nonthermal emission spectra suggests that the radiating particles gain their energy by a stochastic process. Based on an original idea of Fermi [27], the most commonly discussed stochastic acceleration processes fall into two parts: (a) *first order Fermi-acceleration* by diffusive scattering of particles across strong shock waves, also called *shock-acceleration* [28] and (b) *second order Fermi-acceleration*, where the particles gain energy from the scattering at plasma waves [29,30]. Since plasma waves are responsible for the scattering, and thus for the diffusive motion of particles in shock acceleration as well, it is most likely that both processes combine if strong shock waves are present [31]. Fermi acceleration is assumed to be the dominant energy dissipation mechanism in AGN cores and jets, and in gamma-ray bursts. Since Fermi acceleration works independent of particle mass and charge, any protons or ions present at the shock should be accelerated as well as electrons. It has been claimed for various classes of objects that this could be the generating process of the observed cosmic ray spectrum, up to the highest energies of order 10^{20} eV [19]. Here we discuss the maximum energies of protons Fermi-accelerated in emission regions constrained by variability. The time scale for Fermi acceleration is expressed as a multiple of the Larmor time of the particle, $t_{\rm acc}\equiv\theta_{\rm F}t_{\rm L}=2\pi\theta_{\rm F}r_{\rm L}/c$, where we assume $\theta_{\rm F}$ as constant for simplicity; as discussed in Appendix D, this is only true for special assumptions on the diffusion coefficient (e.g., Bohm diffusion). Concerning its magnitude, $\theta_{\rm F}\gg 1$ applies in most cases, but $\theta_{\rm F}\sim 1$ is probably possible for acceleration at relativistic shocks (Appendix D).

1. Larmor radius and adiabatic limits

To be accelerated up to an energy $\hat{E}_p$ by a Fermi mechanism, we have to require that the protons can be magnetically confined in the emission region, viz., $\hat{E}_p\leqslant eBR_{\rm min}$, $R_{\rm min}=\min(R_\parallel,R_\perp)$. Using the relations $R_\parallel<c\mathcal{T}\mathcal{D}$, $E_\nu\leqslant\frac{1}{4}m_\pi c^2\gamma_p$, and $\mathcal{E}_\nu=E_\nu\mathcal{D}$, we obtain the limit

$$\hat{\mathcal{E}}_\nu\leqslant\hat{\mathcal{E}}_{\nu,{\rm L}}=\frac{em_\pi c}{4m_p}B\mathcal{T}\mathcal{D}^2\rho_T\rho_{\rm L}. \tag{14}$$

The factor $\rho_{\rm L}<1$ considers that usually only a limited fraction of the effective size $R_{\rm min}$ of the emission region can practically be used for particle gyration; we assume $\rho_{\rm L}\lesssim\frac{1}{3}$ in the following.

Similar limits can be derived from acceleration time constraints arising from the dynamic time scales involved in the acceleration process. The first condition of this kind is $t_{\rm acc}<T_{\rm inj}$, which can be specified in the internal shock scenario as $t_{\rm L}<T_{\rm cr}/2\theta_{\rm F}\beta_{\rm sh}$, and is obviously equivalent to Eq. (14) with $\rho_{\rm L}=(2\theta_{\rm F}\beta_{\rm sh})^{-1}$. The second condition is the limitation of the acceleration time by adiabatic cooling in a decreasing magnetic field, $t_{\rm acc}<t_{\rm ad}\equiv 2|B/\dot{B}|$. In an expanding emission region, we usually find $B\propto R^{-\alpha}$, where $\alpha>0$ and R is some characteristic size of the emission region. In the general case, in particular for nonisotropic expansion, α may depend on the choice of R; in an isotropically expanding emitter with conserved magnetic energy we have $\alpha=2$, which we may use as a canonical assumption hereafter. Defining the velocity of expansion as $\beta_{\rm ex}\equiv\dot{R}/c$, this results again in Eq. (14), with $\rho_{\rm L}=(\pi\alpha\theta_{\rm F}\beta_{\rm ex})^{-1}$. Adiabatic cooling is most relevant in a freely expanding relativistic fluid, $\beta_{\rm ex}\approx 1$, or for rapidly decaying magnetic fields, $\alpha\gg 1$ (however, we have to assume that the field decay is adiabatic, i.e., $|B/\dot{B}|\gg t_{\rm L}$). For second order Fermi acceleration, both constraints, $t_{\rm acc}<T_{\rm inj}$ and $t_{\rm acc}<t_{\rm ad}$, are equivalent, because the injection time is limited by the adiabatic drop of the Alvén speed, which leads to $T_{\rm inj}\sim t_{\rm ad}$.

In conclusion, Eq. (14) with $\rho_{\rm L}\lesssim\min(\frac{1}{3},\theta_{\rm F}^{-1})$ applies for our canonical assumption that the involved hydrodynamic process is at least transrelativistic. Acceleration time con-

straints then dominate for $\theta_F \gg 1$, which is particularly the case for second order Fermi acceleration, or acceleration at nonrelativistic, quasiparallel shocks (cf. Appendix D), while for any faster acceleration mechanism the geometrical extension of the emission region, constrained by variability, sets the limit on $\mathcal{E}_\nu$.

2. Limits due to radiative cooling

Synchrotron cooling of the protons during acceleration limits their maximum energy through the condition $t_{\rm acc} < t_{p,\rm syn}$. Writing the acceleration time as $t_{\rm acc} = 2\pi\theta_F \gamma_p / \omega_{B,p}$ and using Eq. (3), we find $\gamma_p < 3/\sqrt{8\pi\theta_F\, r_p \omega_{B,p}}$, leading to

$$\hat{\mathcal{E}}_\nu \leqslant \hat{\mathcal{E}}_{\nu,\rm syn(p)} = \frac{3}{8}\frac{m_\pi c^2 \mathcal{D}}{r_p}\sqrt{\frac{e}{2\pi\theta_F B}}. \qquad (15)$$

In the same way, proton acceleration must be faster than the cooling due to photohadronic interactions, $t_{\rm acc} < t_{p\gamma} \approx f_{p\gamma}^{-1} t_{p,\pi}$. To express $t_{b,\pi}$ by observable quantities, we use Eq. (12) to write

$$t_{b,\pi} = \frac{4\pi\mathcal{D}^5 \mathcal{T}^2 \rho_T^2}{\mathrm{T}_\mathcal{L}} \quad \text{with} \quad \mathrm{T}_\mathcal{L} = \frac{\mathcal{L}_b \mathrm{H}_2}{c^2 \varepsilon_b\, x_L (a-1)^2}, \qquad (16)$$

where $\mathcal{L}_b \equiv \mathcal{L}(\varepsilon_b)$ is the isotropic luminosity of the source at the observed spectral break, related to the break energy in the comoving frame by $\varepsilon_b = \epsilon_b \mathcal{D}$, and $\mathrm{H}_2 \approx 22\ \mu$b (cf. Appendix B). Using Eqs. (5a), (5b) we obtain from $t_{\rm acc} < t_{p\gamma}$

$$\hat{\mathcal{E}}_\nu \leqslant \hat{\mathcal{E}}_{\nu,p\gamma} = \frac{m_\pi c^2 \tilde{\gamma}_b}{4}\left[\frac{\omega_{B,p}\mathcal{T}\rho_T}{\theta_F \Upsilon_\mathcal{L} \tilde{\gamma}_b}\right]^{1/a} \mathcal{D}^{2+4/a}$$
$$\text{for} \quad \frac{2\omega_{B,p}\mathcal{T}^2\rho_T^2\mathcal{D}^4}{\theta_F f_{p\gamma} \mathrm{T}_\mathcal{L}} \leqslant \tilde{\gamma}_b, \qquad (17)$$

where we inserted the Doppler scaled characteristic Lorentz factor, $\tilde{\gamma}_b = \epsilon_{\rm th}^{\rm RF}/2\varepsilon_b$, which does not depend on $\mathcal{D}$ and is related to the comoving characteristic Lorentz factor by $\gamma_b = \tilde{\gamma}_b \mathcal{D}$, and

$$\Upsilon_\mathcal{L} = \begin{cases} \mathrm{T}_\mathcal{L}\, f_{p\gamma}/2\mathcal{T}\rho_T & \text{for} \quad \hat{\gamma}_p \lesssim \gamma_b, \\ \mathrm{T}_\mathcal{L}\, f_{p\gamma} N_{\rm ph}/2N_{\rm ph,b}\mathcal{T}\rho_T & \text{for} \quad \hat{\gamma}_p \gg \gamma_b. \end{cases} \qquad (18)$$

The case of Eq. (17) obviously corresponds to $\hat{\gamma}_p \lesssim \gamma_b$; the case $\hat{\gamma}_p \gg \gamma_b$ is described by setting $a=1$ and using the proper value for $\Upsilon_\mathcal{L}$ [note: in Eq. (16), the actual power law index a has to be used in any case]. It should be noted that Eq. (17) only considers the photon density in the burst connected to its intrinsic luminosity. If, however, the relativistically moving ''blob'' is embedded in an ambient photon field, which is isotropic with respect to the observer, the photon density seen in the comoving frame of the blob can be considerably higher than inferred from the observed luminosity by Eq. (12). The reason is, that this additional component would appear unboosted for the observer, and therefore probably only as a small fraction of the apparent luminosity of the emitting blob which is boosted by a factor $\mathcal{D}^4$, while in the comoving frame the photon number density of the *ambient* component is increased by a factor $\mathcal{D}$ due to Lorentz contraction and may thus dominate the photon density. This scenario might be relevant in AGN, if the emission region in the jet is close to the AGN core, and if the core radiation is isotropized by a plasma halo (see, e.g., [32]), and photohadronic interactions may limit the neutrino energy to values significantly below the upper limit expressed by Eq. (17).

C. Cooling of secondary particles in the hadronic cascade

1. Cooling processes and time scales

Pions and muons are weakly decaying particles, with comparatively long lifetimes, $\tau_\pi^{\rm RF} = 2.6\times10^{-8}$ s and $\tau_\mu^{\rm RF} = 2.2\times10^{-6}$ s, respectively. For secondary particle Lorentz factors $\gamma_\star^{\rm pr} \approx \gamma_p \gtrsim 10^{6-8}$, which are quite reasonable and readily considered in most models, their lifetime in the comoving frame of the emission region, $\tau_\star = \tau_\star^{\rm RF}\gamma_\star$, can be of the order the dynamical time scale of the flare (e.g., in gamma-ray bursts). Moreover, their synchrotron losses are by a factor $(m_p/m_\star)^3 \sim 10^3$ stronger than for protons. Adiabatic cooling of muons has been considered for neutrino emission of gamma-ray bursts [14], and synchrotron cooling of pions and muons has been discussed for extremely magnetized environments, e.g., neutron star magnetospheres [33]. Most of the literature about neutrino emission of AGN, however, neglects this effect. We will show here that this is not justified, and derive the critical Lorentz factors, $\tilde{\gamma}_\star$, above which the energy loss of muons and pions plays a role. Obviously, we have to distinguish between neutrinos from the decay of pions and muons, because of their very different lifetimes. Energy losses of the muons are generally more relevant, which affects in particular the electron neutrinos, arising exclusively from muon decay. This is important for neutrino detection in UHE air shower experiments, where electron neutrino showers are easier to distinguish from the atmospheric background and are therefore proposed as providing most of the expected signal [12,34].

Secondary particles cool adiabatically prior to their decay if $\tau_\star > 2|B/\dot{B}|$, which gives a critical Lorentz factor $\tilde{\gamma}_\star = 2R/\alpha\beta_{\rm ex}\tau_\star^{\rm RF}$ for $B \propto R^{-\alpha}$, leading to

$$\tilde{\mathcal{E}}_{\nu,\rm ad(\star)} = E_{\nu,\star}^{\rm RF}\frac{2\rho_T\mathcal{T}\mathcal{D}^2}{\alpha\beta_{\rm ex}\tau_\star^{\rm RF}}, \qquad (19)$$

where $E_{\nu,\star}^{\rm RF}$ is the neutrino energy in the rest frame of the decaying particle, which is roughly $\frac{1}{4}m_\pi c^2 \approx 35$ MeV for the pion decay, but slightly smaller (30 MeV) for muon decay and may therefore be distinguished (see Appendix B). Analogously, pions and muons can undergo efficient synchrotron cooling if $\tau_\star \leqslant t_{\star,\rm syn}$. The critical Lorentz factor is thus found from $\gamma_b t_{b,\rm syn}(m_\star/m_p)^3 = \tilde{\gamma}_\star^2 \tau_\star^{\rm RF}$, yielding

$$\tilde{\mathcal{E}}_{\nu,\rm syn(\star)} = \frac{\omega_\star}{\omega_{B,\star}} E_{\nu,\star}^{\rm RF}\mathcal{D} \quad \text{with} \quad \omega_\star = \frac{3}{2}\sqrt{\frac{c}{\tau_\star^{\rm RF} r_\star}}, \qquad (20)$$

where $r_\star = e^2/m_\star c^2$ is the classical radius of the particle, and $\omega_{B,\star} = eB/m_\star c$ its cyclotron frequency. The characteristic

frequency, $\omega_\star$, for synchrotron losses of pions and muon is found as $\omega_\pi = 5.0\times 10^{16}$ s^{-1} and $\omega_\mu = 4.7\times 10^{15}$ s^{-1}, respectively. Secondary particles may also suffer inverse Compton (IC) losses from interactions with background photons. The corresponding cooling time is related to the synchrotron cooling time by the well known relation

$$t_{\star,\mathrm{IC}} = t_{\star,\mathrm{syn}} \frac{u_{\mathrm{ph}}}{u_B} \approx t_{\star,\mathrm{syn}} \frac{2 L_b b_{\mathrm{ph}}}{B^2 R_\parallel^2 c x_L}, \tag{21}$$

where b_{ph} is the bolometric correction factor relating the total photon luminosity over the spectral range ϵ_{b} to $\hat{\epsilon}$ to L_{b} given by $b_{\mathrm{ph}} = |(\hat{\epsilon}/\epsilon_{\mathrm{b}})^{2-a} - 1|/|2-a|$ for $a \neq 2$, and $b_{\mathrm{ph}} \approx \ln(\hat{\epsilon}/\epsilon_{\mathrm{b}})$ for $a = 2$. For high pion and muon energies Eq. (21) might be modified by Klein-Nishina corrections, leading to a suppression of IC cooling.

Unlike the proton case, IC cooling is the most relevant process for photointeractions of pions and muons. Their IC cooling time is related to the proton IC cooling time as $t_{\star,\mathrm{IC}} = (m_\star/m_p)^3 t_{p,\mathrm{IC}}$, while the Bethe-Heitler cooling time only scales with $t_{\star,\mathrm{BH}} = (m_\star/m_p) t_{p,\mathrm{BH}}$. For $a = 2$, one can show that $t_{\star,\mathrm{BH}} \sim 5 t_{\star,\mathrm{IC}}$, if Klein-Nishina corrections are disregarded. For the pion, there are additional channels due to meson resonance excitation; the lowest energy process is $\pi^\pm \gamma \to \rho^\pm \to \pi^\pm \pi^0$, which has a theoretical peak cross section of ~ 50 μb (determined from the $\rho^\pm \to \pi^\pm \gamma$ decay branching ratio by use of the Breit-Wigner formula [35]), at a photon energy of $\epsilon_{\pi\to\rho} \sim 2$ GeV in the pion rest frame. Compared to the pion production off the proton via the Δ-resonance, where the characteristic photon energy is $\epsilon_{p\to\Delta} \sim 300$ MeV, this interaction is suppressed by a factor $\sim \frac{1}{6}(\epsilon_{p\to\Delta}/\epsilon_{\pi\to\rho})^a$; for $a \approx 2$, and neglecting the finite lifetime of the pion, secondary photon scattering has a probability of $<0.3\%$, and can thus be neglected. However, the process may be relevant in inverted photon spectra, e.g., for pion production in the Rayleigh-Jeans part of the thermal background.

2. Spectral modification at the critical energies

The ''maximum'' neutrino energies derived in Sec. III B arise from the balance of energy gain and loss processes. The stochastic nature of these processes allows the particles to exceed such ''limits'' with some, usually exponentially decreasing probability. This has been shown for Fermi accelerated particles subject to synchrotron losses [36], which show a largely unmodified extension of the power law spectrum up to the cutoff energy (defined by balance of gains and losses), followed by an exponential-like cutoff; depending on the detailed parameters, a pile-up may occur at the cutoff energy. Although the stochastic behavior of photohadronic losses is quite different from synchrotron losses, we may expect a similar result in this case, and also for adiabatic losses. In general, we can assume that if the neutrino energy is limited by the maximum proton energy, the spectrum will continue as an approximate power law up to $\hat{\mathcal{E}}_\nu$, and drop off rapidly for $\mathcal{E}_\nu > \hat{\mathcal{E}}_\nu$.

The situation is different for the decay of unstable particles, where the particle can decay within a time Δt after its production with a probability $P_{\mathrm{dc}} = 1 - \exp(-\Delta t/\tau_\star)$. Far above the critical Lorentz factor, $\gamma_\star^{\mathrm{dc}} \gg \tilde{\gamma}_\star$, the decay probability within a cooling time scale in the fluid frame, $\Delta t = t_{\mathrm{cool}}(\gamma_\star) \ll \tau_\star$, can be approximated as $P_{\mathrm{dc}}(t_{\mathrm{cool}}) \approx t_{\mathrm{cool}}(\gamma_\star)/\tau_\star$. The critical Lorentz factor is defined by the condition that $t_{\mathrm{cool}}(\tilde{\gamma}_\star) = \tilde{\gamma}_\star \tau_\star^{\mathrm{RF}}$, which allows us to write $t_{\mathrm{cool}}(\gamma_\star) = \tau_\star (\gamma_\star/\tilde{\gamma}_\star)^{-w}$. For adiabatic cooling, $t_{\mathrm{cool}} = \mathrm{const}(\gamma_\star)$ then means $w = 1$, while for synchrotron cooling we have $w = 2$; cooling by secondary photon scattering—if relevant—would correspond to $w = a$. For pions or muons produced with $\gamma_\star^{\mathrm{pr}} \lesssim \tilde{\gamma}_\star$, neutrinos are produced with an energy $\mathcal{E}_\nu \approx E_{\nu,\star}^{\mathrm{RF}} \gamma_p \mathcal{D}$ in the observers frame, and their power spectrum is $\mathcal{L}_\nu \propto \mathcal{E}_\nu^{\,q}$, as discussed in Sec. II B. For $\gamma_\star^{\mathrm{pr}} \gg \tilde{\gamma}_\star$, the power spectrum is modified by the probability to decay within a cooling time $t_{\mathrm{cool}}(\gamma_\star^{\mathrm{pr}})$, viz.,

$$\begin{aligned} \overline{\mathcal{L}}_\nu &\propto \mathcal{E}_\nu^{\,q} P_{\mathrm{dc}}(t_{\mathrm{cool}})\big|_{\gamma_\star = \mathcal{E}_\nu/\mathcal{D}E_{\nu,\star}^{\mathrm{RF}}} \\ &\propto \mathcal{E}_\nu^{\,q-w} \quad \text{for } \mathcal{E}_\nu \gg E_{\nu,\star}^{\mathrm{RF}} \tilde{\gamma}_\star \mathcal{D}. \end{aligned} \tag{22}$$

Therefore, the critical Lorentz factor marks a spectral break of magnitude $\Delta q = -w$, rather than an exponential cutoff. Clearly, this simplified analytical estimate does not treat exactly the energy evolution of the pions and muons, thus neglects particle number conservation. Considering this would lead to a pile-up of decaying pions and muons around their respective critical Lorentz factor, before the spectrum turns over into a $\mathcal{E}_\nu^{\,q-w}$ behavior. The strength of the pile-up is correlated to the magnitude of the spectral break, and is therefore expected to be stronger for synchrotron cooling breaks than for adiabatic cooling breaks. The break due to adiabatic cooling of secondary particles is comparable to the spectral breaks occurring at the transition between different dominant proton cooling processes, Eq. (9a). The $\Delta q = -2$ break caused by pion or muon synchrotron cooling, however, is stronger and can be easily confused with an exponential steepening: it causes a drop of events of one order of magnitude over half a decade in energy, similar to the exponential function around its critical energy. In practice, we may therefore consider $\tilde{\mathcal{E}}_{\nu,\mathrm{syn}(\star)}$, as a cutoff energy of the neutrino spectrum and compare it with with the cutoff energies due to proton cooling as derived in Sec. III B.

D. Model-independent discussion of spectral shapes, maximum energies and fluxes

1. The parameter space

The free parameters describing a transient fall into two classes: (i) observable parameters, i.e., the characteristic time scale, $\mathcal{T}$, and the isotropized luminosity, $\mathcal{L}$, and (ii) theoretical parameters, like B, $\mathcal{D}$, θ_{F}, etc. We consider the former as given for any specific transient (disregarding possible problems in their determination, cf. Sec. III A 2), while the latter can only be constrained through general physical considerations or additional observations within a certain range. Equations (14), (15), and (17) show that the maximum energies depend strongly on some of these parameters, in particular on the magnetic field B and the Doppler factor $\mathcal{D}$.

In contrast, the hydrodynamic parameters of the flow, i.e., α, $\beta_{\rm ex}$ and $\beta_{\rm sh}$ are of order unity, and can generally be recast into some reasonable assumption for $\rho_{\rm L}$. A special role is played by $\theta_{\rm F}$, which describes the speed of the acceleration process: as shown in Appendix D, first and second order Fermi acceleration is limited to $\theta_{\rm F}>1$, but we could easily consider any faster acceleration process in our analysis by inserting the appropriate $\theta_{\rm F}$. We therefore shall use $\theta_{\rm F}$ as a fixed parameter, with the canonical assumption that $\theta_{\rm F}\approx 1$, while B and $\mathcal{D}$ span the two-dimensional parameter space describing a transient. From Eqs. (14), (15), and (17) we can immediately derive a qualitative division of the parameter space.

(1) For any given $\mathcal{D}$, synchrotron losses of protons dominate over both photohadronic or adiabatic (Larmor) limits for magnetic fields larger than some value $\check{B}_{\rm syn(p)}(\mathcal{D})$. Analogously, there is a magnetic field $\check{B}_{\rm syn(\star)}(\mathcal{D})$ above which muon or pion synchrotron losses dominate over all other proton loss processes; the relation of $\check{B}_{\rm syn(p)}(\mathcal{D})$ and $\check{B}_{\rm syn(\star)}(\mathcal{D})$ depends on the other parameters.

(2) For any given B, photohadronic interactions of protons dominate over both synchrotron and adiabatic (Larmor) limits for Doppler factors smaller than some value $\hat{\mathcal{D}}_{p\gamma}(B)$. Similarly, there is a limit $\hat{\mathcal{D}}_{p\gamma,\star}$ below which photohadronic interactions also dominate over pion or muon synchrotron cooling.

(3) For any given $\mathcal{D}$, there is a limiting magnetic field $\check{B}_{\rm ad(p)}(\mathcal{D})$ below which adiabatic or Larmor limits dominate over synchrotron or photohadronic cooling of protons, and another value $\check{B}_{\rm ad(\star)}$ below which it dominates over either muon or pion synchrotron cooling.

It is much more difficult to determine under which conditions adiabatic cooling of secondary particles dominates; we will see in Sec. IV B that, if at all, this can happen only in a very limited region of the parameter space. For a more illustrative discussion of the parameter space constraints specific to AGN jets and gamma-ray bursts see Sec. IV A 2 and Sec. IV B 2, and the figures shown there.

To get a quantitative idea about the above parameter space division, we derive the condition under which the delimiting energies $\hat{\mathcal{E}}_{\nu,{\rm syn}(p)}$, $\hat{\mathcal{E}}_{\nu,p\gamma}$, and $\hat{\mathcal{E}}_{\nu,{\rm L}}$ are all equal. This is equivalent to the condition $t_{\rm acc}=t_{p,{\rm syn}}=t_{p\gamma}=2\pi\rho_{\rm L}\theta_{\rm F}R/c$, representing three equations which can be solved for the three variables B, $\mathcal{D}$ and γ_p; note that the latter term reduces to $2R/c\alpha\beta_{\rm ex}=t_{\rm ad}$ in the case $\rho_{\rm L}=(\pi\alpha\beta_{\rm ex}\theta_{\rm F})^{-1}$, i.e., that adiabatic cooling rather than space limitations determines the Larmor limit. The corresponding solutions for the magnetic field, Doppler factor, and maximum proton Lorentz factor are called B^*, $\mathcal{D}^*$, and $\hat{\gamma}_p^*$, respectively, and are for the case $\hat{\gamma}_p\leqslant\gamma_{\rm b}$ given as

$$\mathcal{D}^*=[\Upsilon_{\mathcal{L}}^3\Upsilon_{\mathcal{T}}^{a-1}\rho_{\rm L}^{a+2}\theta_{\rm F}^{4-a}]^y \tag{23a}$$

$$B^*=B_{\rm b}[\Upsilon_{\mathcal{L}}\Upsilon_{\mathcal{T}}^{a+3}\rho_{\rm L}^{a+4}\theta_{\rm F}^3]^{-2y} \tag{23b}$$

$$\hat{\gamma}_p^*=\tilde{\gamma}_{\rm b}[\Upsilon_{\mathcal{L}}\Upsilon_{\mathcal{T}}^{a+3}\rho_{\rm L}^{a+4}\theta_{\rm F}^{-(a+2)}]^y, \tag{23c}$$

with $y=(2a+10)^{-1}$, where we introduced the magnetic field scale $B_{\rm b}=9m_p^2c^4/8\pi e^3\tilde{\gamma}_{\rm b}^2=[7.3\times10^{21}\ {\rm G}]\tilde{\gamma}_{\rm b}^{-2}$, and the dimensionless quantity

$$\Upsilon_{\mathcal{T}}\equiv\frac{9}{8\pi}\frac{c\mathcal{T}\rho_T}{r_p\tilde{\gamma}_{\rm b}^3}. \tag{24}$$

The relations for the case $\hat{\gamma}_p\gg\gamma_{\rm b}$ are obtained from Eqs. (23) by setting $a=1$ and use the proper value of $\Upsilon_{\mathcal{L}}$ from Eq. (18). The corresponding maximum neutrino energy is obviously given as $\hat{\mathcal{E}}_\nu^*=\frac{1}{4}m_\pi c^2\mathcal{D}^*\hat{\gamma}_p^*$. Equations (23) define a unique reference point in the parameter space of magnetic field and Doppler factor, which allows the discussion of the relation of cooling processes of the proton independent of any other physical properties of the transient; for notational simplicity, we refer to it as the *star-point* hereafter.

For some applications it is useful to normalize the magnetic field energy density by the comoving photon energy density. We introduce the equipartition parameter

$$\xi_{B\gamma}\equiv\frac{u_B}{u_{\rm ph}}=\frac{c^3\rho_T^2\mathcal{T}^2x_{\rm L}B^2\mathcal{D}^6}{2b_{\rm ph}\mathcal{L}_{\rm b}}, \tag{25}$$

where $b_{\rm ph}$ is the bolometric correction factor of the photon spectrum as defined in Eq. (21). Without protons, $\xi_{B\gamma}\sim1$ would correspond to approximate energy equipartition of magnetic field and relativistic particles, $u_B\sim u_e\sim u_{\rm ph}$, because of the high radiative efficiency of electrons. In baryon loaded flows this is not generally the case because of the contribution of relativistic protons with low radiative efficiency, and $u_p+u_e\sim u_B$ may imply $\xi_{B\gamma}\gg1$ if the acceleration process works more efficiently for protons. The corresponding star-point value is

$$\xi_{B\gamma}^*=\frac{m_pc^3\tilde{\gamma}_{\rm b}^2x_{\rm L}}{2b_{\rm ph}\mathcal{L}_{\rm b}r_p}[\Upsilon_{\mathcal{L}}^7\Upsilon_{\mathcal{T}}^{3a+1}\rho_{\rm L}^{a-2}\theta_{\rm F}^{6-3a}]^{2y}. \tag{26}$$

2. General upper limits on the neutrino energy

For any given Doppler factor, the highest neutrino energy can be achieved for $B=\check{B}_{\rm syn(p)}(\mathcal{D})$, because with increasing B, $\hat{\mathcal{E}}_{\nu,{\rm L}}$ increases and $\hat{\mathcal{E}}_{\nu,p\gamma}$ remains constant, while $\hat{\mathcal{E}}_{\nu,{\rm syn}(p)}$ decreases. The equations determining $\check{B}_{\rm syn(p)}$ are $\hat{\mathcal{E}}_{\nu,{\rm L}}=\hat{\mathcal{E}}_{\nu,{\rm syn}(p)}$ for $\mathcal{D}<\mathcal{D}^*$ and $\hat{\mathcal{E}}_{\nu,p\gamma}=\hat{\mathcal{E}}_{\nu,{\rm syn}(p)}$ for $\mathcal{D}\geqslant\mathcal{D}^*$, leading to

$$\check{B}_{\rm syn(p)}=B^*(\mathcal{D}/\mathcal{D}^*)^{-k}\quad\text{for}\quad\mathcal{D}<\mathcal{D}^* \tag{27a}$$

$$\check{B}_{\rm syn(p)}=B^*(\mathcal{D}/\mathcal{D}^*)^{-2/3}\quad\text{for}\quad\mathcal{D}\geqslant\mathcal{D}^*, \tag{27b}$$

with $k=2+4/(a+2)$ in the case $\hat{\gamma}_p\lesssim\gamma_{\rm b}$, and $k=\frac{10}{3}$ for $\hat{\gamma}_p\gg\gamma_{\rm b}$. If we use $\xi_{B\gamma}$ as a coordinate of the parameter space instead of B, and the maximum neutrino energy is reached for $\check{\xi}_{B\gamma,{\rm syn(p)}}=\xi_{B\gamma}^*(\mathcal{D}/\mathcal{D}^*)^{14/3}$ for $\mathcal{D}>\mathcal{D}^*$, and $\check{\xi}_{B\gamma,{\rm syn(p)}}=\xi_{B\gamma}^*(\mathcal{D}/\mathcal{D}^*)^{6-2k}$ otherwise. This provides an upper limit for the maximum neutrino energy as a function of $\mathcal{D}$

$$\hat{\mathcal{E}}_\nu \leqslant \hat{\tilde{\mathcal{E}}}_{\nu,p}(\mathcal{D}) = \hat{\mathcal{E}}^*_\nu (\mathcal{D}/\mathcal{D}^*)^{1+k/2} \quad \text{for} \quad \mathcal{D} < \mathcal{D}^* \tag{28a}$$

$$\hat{\mathcal{E}}_\nu \leqslant \hat{\tilde{\mathcal{E}}}_{\nu,p}(\mathcal{D}) = \hat{\mathcal{E}}^*_\nu (\mathcal{D}/\mathcal{D}^*)^{4/3} \quad \text{for} \quad \mathcal{D} \geqslant \mathcal{D}^*. \tag{28b}$$

Stronger constraints on $\hat{\mathcal{E}}_\nu$ may exist from secondary particle cooling. We will only consider synchrotron cooling, because the impact of adiabatic cooling of secondary particles on the neutrino spectral shape is relatively weak, as argued in Sec. III C 2; moreover, it is often dominated by the other cooling processes, as we will see in Sec. IV. From the conditions $\tilde{\mathcal{E}}_{\nu,\mathrm{syn}(\star)} = \hat{\mathcal{E}}_{\nu,p\gamma}$ for $\mathcal{D} \lesssim \mathcal{D}^*$, and $\tilde{\mathcal{E}}_{\nu,\mathrm{syn}(\star)} = \hat{\mathcal{E}}_{\nu,\mathrm{L}}$ otherwise, we find the solutions for the magnetic field

$$\check{B}_{\mathrm{syn}(\star)}(\mathcal{D}) \approx \check{B}^*_{\mathrm{syn}(\star)} (\mathcal{D}/\mathcal{D}^*)^{-k_\star} \quad \text{for} \quad \mathcal{D} \lesssim \mathcal{D}^* \tag{29a}$$

$$\check{B}_{\mathrm{syn}(\star)}(\mathcal{D}) = \check{B}^*_{\mathrm{syn}(\star)} (\mathcal{D}/\mathcal{D}^*)^{-1/2} \quad \text{for} \quad \mathcal{D} \gtrsim \mathcal{D}^*, \tag{29b}$$

where $k_\star = 1 + 3/(a+1)$, and $\check{B}^*_{\mathrm{syn}(\star)} = \sqrt{B_{\mathcal{T}} B_\star / \rho_{\mathrm{L}} \mathcal{D}^*}$ with $B_{\mathcal{T}} \equiv m_p c / e \rho_T \mathcal{T}$ and $B_\star \equiv m_\star \omega_\star c / e$. Using $\xi_{B\gamma}$ as a variable, we obtain $\xi_{B\gamma} \approx \check{\xi}^*_{B\gamma,\mathrm{syn}(\star)} (\mathcal{D}/\mathcal{D}^*)^{6-2k_\star}$ and $\xi_{B\gamma} = \check{\xi}^*_{B\gamma,\mathrm{syn}(\star)} (\mathcal{D}/\mathcal{D}^*)^5$, respectively, with

$$\check{\xi}^*_{B\gamma,\mathrm{syn}(\star)} = \frac{c^3 \rho_T^2 \mathcal{T}^2 x_L B_{\mathcal{T}} B_\star \mathcal{D}^{*5}}{2 \rho_{\mathrm{L}} b_{\mathrm{ph}} \mathcal{L}_{\mathrm{b}}}. \tag{30}$$

The transition from photohadronic to adiabatic dominance at $B = \check{B}_{\mathrm{syn}(\star)}(\mathcal{D})$ is exactly at $\mathcal{D} = \mathcal{D}^*$ in the case $\hat{\gamma}_p \gg \gamma_{\mathrm{b}}$. For $\hat{\gamma}_p \leqslant \gamma_{\mathrm{b}}$ the exact transition value could be easily found by setting Eq. (29a) and Eq. (29b) equal and solving for $\mathcal{D}$, but the approximate division at $\mathcal{D}^*$ will usually be adequate in practice. Secondary particle cooling determines the maximum energy in the case $\check{B}_{\mathrm{syn}(\star)}(\mathcal{D}) < \check{B}_{\mathrm{syn(p)}}(\mathcal{D})$, and the corresponding upper limits to the neutrino energy are

$$\hat{\mathcal{E}}_\nu \leqslant \hat{\tilde{\mathcal{E}}}_{\nu,\star}(\mathcal{D}) = \hat{\tilde{\mathcal{E}}}_{\nu,\star}(\mathcal{D}^*) (\mathcal{D}/\mathcal{D}^*)^{k_\star + 1} \quad \text{for} \quad \mathcal{D} \lesssim \mathcal{D}^* \tag{31a}$$

$$\hat{\mathcal{E}}_\nu \leqslant \hat{\tilde{\mathcal{E}}}_{\nu,\star}(\mathcal{D}) = \hat{\tilde{\mathcal{E}}}_{\nu,\star}(\mathcal{D}^*) (\mathcal{D}/\mathcal{D}^*)^{3/2} \quad \text{for} \quad \mathcal{D} \gtrsim \mathcal{D}^*, \tag{31b}$$

with

$$\hat{\tilde{\mathcal{E}}}_{\nu,\star}(\mathcal{D}^*) = E^{\mathrm{RF}}_{\nu,\star} \sqrt{\rho_{\mathrm{L}} \rho_T \mathcal{T} m_\star \omega_\star \mathcal{D}^{*3} / m_p}. \tag{31c}$$

Obviously, $\mathcal{D}^*$ can be replaced by any reference Doppler factor in Eq. (31b). A more illustrative discussion of the relation between $\check{B}_{\mathrm{syn}(\star)}(\mathcal{D})$ and $\check{B}_{\mathrm{syn(p)}}(\mathcal{D})$ in the different regions of the parameter space is given in Sec. IV.

3. Efficiency considerations and neutrino flux limits

Relevant for the observability of ultra-high energy neutrinos is not only the maximum neutrino energy a specific class of sources can provide, but also which total neutrino luminosity is associated to this energy. This requires a discussion of the neutrino efficiency as a function of the parameter space.

If we assume that $B < \check{B}_{\mathrm{syn}(\star)}$, i.e., we are in the part of the parameter space where secondary particle cooling plays no role, then the neutrino efficiency can be written as $\zeta_\nu = \frac{1}{2} \overline{t_p} / t_{p,\pi}$, which can be rewritten as $\zeta_\nu = \frac{1}{2} f^{-1}_{\mathrm{max}}$ if one cooling process clearly dominates. In the star-point, where all cooling times are equal at the maximum proton energy, the neutrino efficiency at this energy is most easily derived as $\zeta^*_\nu = (6 f^*_{p\gamma})^{-1}$, with $f^*_{p\gamma} \approx 3 + \exp(5a - 10)$ since both terms for neutron reconversion in Eq. (6) are small in the star-point. Using the scaling properties of the cooling times, we can then derive the following simple expressions.

If photohadronic cooling dominates,

$$\xi_\nu \approx \frac{1}{2} f^{-1}_{p\gamma,\mathrm{min}} \quad \text{with} \quad f_{p\gamma,\mathrm{min}} \approx 1 + \exp(5a - 10), \tag{32a}$$

which leads to $\hat{\zeta}_{\nu,\mathrm{ad}} \approx \frac{1}{2}$ if $a \leqslant 2$, i.e., if Bethe-Heitler losses can be neglected. In general, the total hadronic radiative efficiency in this region is ≈ 1, which approximately equal parts (for $a \leqslant 2$) radiated in neutrino and electromagnetic channels. Cosmic ray ejection is generally suppressed by neutron reabsorption, and direct proton ejection can usually be assumed to be marginal, except for special geometries and, maybe, at the highest energies.

If adiabatic cooling dominates,

$$\zeta_\nu \approx 3 \zeta^*_\nu \left(\frac{\mathcal{D}}{\mathcal{D}^*} \right)^{-(3+a)} \left(\frac{\gamma_p}{\hat{\gamma}^*_p} \right)^{a-1}, \tag{32b}$$

where ζ^*_ν is the efficiency at the star-point. Here, most of the energy is not radiated, but reconverted into kinetic energy of expansion. Thus, the total hadronic radiative energy decreases in total, while the distribution of the radiated energy between cosmic rays, neutrinos and photons remains constant, and approximately 2:1:1 for $a \leqslant 2$.

If synchrotron cooling dominates,

$$\zeta_\nu \approx 3 \zeta^*_\nu \left(\frac{f^*_{p\gamma}}{f_{p\gamma}} \right) \left(\frac{B}{B^*} \right)^{-2} \left(\frac{\mathcal{D}}{\mathcal{D}^*} \right)^{-(4+a)} \left(\frac{\gamma_p}{\hat{\gamma}^*_p} \right)^{a-2}. \tag{32c}$$

Like in the case of photohadronic dominance, the total hadronic radiative efficiency is close to 1, but the predominant part of the energy is emitted in electromagnetic radiation. The correction factor $1 \leqslant f^*_{p\gamma} / f_{p\gamma} < 3$ considers that in the region of synchrotron dominance neutron reabsorption may or may not play a role, depending on the ratio of the photohadronic interaction time scale to the crossing time.

Note that, instead of the star-point, any point in or at the border of the respective dominance region could be used as a reference point in Eqs. (32). If secondary particle cooling plays a role, the situation is similar: For synchrotron cooling, the total hadronic radiative efficiency remains constant, but more energy is channeled into energetic photons; for adiabatic cooling, additional energy is reconverted in bulk kinetic energy. We do not discuss the scaling properties for these cases; rather, we will use $\tilde{\mathcal{E}}_{\nu,\mathrm{syn}(\star)}$ as limiting energy and discuss the efficiencies only for $\mathcal{E}_\nu < \tilde{\mathcal{E}}_{\nu,\mathrm{syn}(\star)}$, and neglect the effect of adiabatic cooling of secondary particles altogether.

The neutrino efficiency alone does not allow to derive flux rates; we also have to make assumptions about the en-

ergy density of relativistic protons in the source. Here we can use the standard equipartition argument discussed above, and introduce a parameter $\overline{\xi}_{pB} \equiv \overline{u}_p / u_B \sim 1$, which allows us to express the time integrated proton injection energy density, $\overline{u}_p$ by the parameter space variable $\xi_{B\gamma}$ defined in Eq. (25). The neutrino luminosity at the maximum energy can then be expressed relative to the bolometric photon luminosity as $\ell_\nu \equiv \overline{\mathcal{L}}_\nu / b_{\rm ph}\mathcal{L}_{\rm b}\mathcal{T}$, and we define

$$\hat{\hat{\ell}}_\nu \equiv \left. \frac{\overline{\mathcal{L}}_\nu}{b_{\rm ph}\mathcal{L}_{\rm b}\mathcal{T}} \right|_{\mathcal{E}_\nu = \hat{\hat{\mathcal{E}}}_\nu(\mathcal{D})} = \left. \frac{\overline{\xi}_{pB}\xi_{B\gamma}\zeta_\nu}{b_p} \right|_{\gamma_p = \hat{\hat{\gamma}}_p(\mathcal{D})}, \qquad (33)$$

where $\hat{\hat{\gamma}}_p$ denotes the maximum proton Lorentz factor attainable for a given $\mathcal{D}$ for which secondary particle cooling can yet be neglected. If $\check{B}_{\rm syn(\star)}(\mathcal{D}) > \check{B}_{\rm syn(p)}(\mathcal{D})$, $\xi_{B\gamma}$ and $\zeta_\nu(\hat{\gamma}_p)$ have to be evaluated at $B = \check{B}_{\rm syn(p)}(\mathcal{D})$ and we obtain

$$\hat{\hat{\ell}}_{\nu,p} = \frac{\overline{\xi}_{pB}\xi^*_{B\gamma}}{4 b_p\, f_{p\gamma,\rm min}} \left(\frac{\mathcal{D}}{\mathcal{D}^*} \right)^{(2a-4)/(a+2)} \quad \text{for } \mathcal{D} < \mathcal{D}^* \qquad (34a)$$

$$\hat{\hat{\ell}}_{\nu,p} = \frac{\overline{\xi}_{pB}\xi^*_{B\gamma}}{4 b_p\, f^*_{p\gamma}} \left(\frac{\mathcal{D}}{\mathcal{D}^*} \right)^{(4-2a)/3} \quad \text{for } \mathcal{D} > \mathcal{D}^*, \qquad (34b)$$

while for $\mathcal{D} = \mathcal{D}^*$ we have $\hat{\hat{\ell}}_{\nu,p} = \ell^*_\nu \equiv \overline{\xi}_{pB}\xi^*_{B\gamma}/6 b_p f^*_{p\gamma}$. If $\check{B}_{\rm syn(\star)}(\mathcal{D}) < \check{B}_{\rm syn(p)}(\mathcal{D})$, $\xi_{B\gamma} = \xi_{B\gamma,\rm syn(\star)}(\mathcal{D})$ has to be used to determine $\hat{\hat{\gamma}}_p(\mathcal{D})$, leading to

$$\hat{\hat{\ell}}_{\nu,\star} \approx \frac{\overline{\xi}_{pB}\check{\xi}^*_{B\gamma,\rm syn(\star)}}{4 b_p\, f_{p\gamma,\rm min}} \left(\frac{\mathcal{D}}{\mathcal{D}^*} \right)^{(4a-2)/(a+1)} \quad \text{for } \mathcal{D} < \mathcal{D}^* \qquad (35a)$$

$$\hat{\hat{\ell}}_{\nu,\star} \approx \frac{\overline{\xi}_{pB}\check{\xi}^*_{B\gamma,\rm syn(\star)}}{4 b_p\, f^*_{p\gamma}} \left(\frac{\mathcal{D}}{\mathcal{D}^*} \right)^{(3-a)/2} \quad \text{for } \mathcal{D} \geq \mathcal{D}^*. \qquad (35b)$$

We note that, if secondary particle cooling plays no role, $\hat{\hat{\ell}}_\nu$ is independent of $\mathcal{D}$ for $a = 2$, and has a maximum for $\mathcal{D} = \mathcal{D}^*$ for $a > 2$. In case of the dominance of secondary particle cooling, a maximum is only obtained for $a \geq 3$, while otherwise $\hat{\hat{\ell}}_\nu$ continues to rise with $\mathcal{D}$. Therefore, for given $\mathcal{L}_{\rm b}$, both the maximum neutrino energy and the power flux at this energy increases with $\mathcal{D}$ in most cases, and a general upper limit cannot be stated. However, we have to consider that increasing $\mathcal{D}$, while maintaining $\hat{\gamma}_p = \hat{\hat{\gamma}}_p$, implies that also $\xi_{B\gamma}$ and therefore the total energy dissipated into relativistic particles and magnetic fields by the transient, $\mathfrak{E}_{\rm T}$, increases. Since $\mathfrak{E}_{\rm T}$ is usually given, or at least limited by fundamental principles for any specific kind of source model, we can impose an upper limit

$$\xi_{B\gamma} < \xi_{B\gamma,\rm max} \equiv \frac{1}{(1+\overline{\xi}_{pB})} \left(\frac{4\pi}{\Omega} \frac{\mathfrak{E}_T}{b_{\rm ph}\mathcal{L}_{\rm b}\mathcal{T}} - 1 \right), \qquad (36)$$

where Ω is the total angle over which the energy is emitted; the case of emission in a thin, freely expanding jet corresponds to $\Omega \approx \mathcal{D}^{-2}$. This can be transformed into an upper limit on the Doppler factor for which both $\hat{\mathcal{E}}_\nu = \hat{\hat{\mathcal{E}}}_\nu$ and $\overline{\mathcal{L}}_\nu(\hat{\mathcal{E}}_\nu) = \hat{\ell}_\nu b_{\rm ph}\mathcal{L}_{\rm b}\mathcal{T}$ can be attained, which we call $\hat{\hat{\mathcal{D}}}$; for simplicity, we confine the discussion to the case $\xi_{B\gamma,\rm max} > \check{\xi}^*_{B\gamma,\rm syn(\star)}$, which means $\hat{\hat{\mathcal{D}}} > \mathcal{D}^*$, and assume $\xi_{B\gamma,\rm max} \gg 1$. From Eq. (31b) we then obtain a general, model-independent upper limit on the neutrino energy as

$$\hat{\hat{\mathcal{E}}}_\nu \leq \hat{\hat{\mathcal{E}}}_{\nu,p}(\hat{\hat{\mathcal{D}}}) = \hat{\mathcal{E}}^*_\nu \left[\frac{4\pi\mathfrak{E}_{\rm T}}{\Omega^* b_{\rm ph}\mathcal{L}_{\rm b}\mathcal{T}(1+\overline{\xi}_{pB})\xi^*_{B\gamma}} \right]^{\kappa_p} \quad \text{for } \check{B}_{\rm syn(\star)}(\hat{\hat{\mathcal{D}}}) \geq \check{B}_{\rm syn(p)}(\hat{\hat{\mathcal{D}}}) \qquad (37a)$$

$$\hat{\hat{\mathcal{E}}}_\nu \leq \hat{\hat{\mathcal{E}}}_{\nu,\star}(\hat{\hat{\mathcal{D}}}) = \hat{\hat{\mathcal{E}}}_{\nu,\star}(\mathcal{D}^*) \left[\frac{4\pi\mathfrak{E}_{\rm T}}{\Omega^* b_{\rm ph}\mathcal{L}_{\rm b}\mathcal{T}(1+\overline{\xi}_{pB})\check{\xi}^*_{B\gamma,\rm syn(\star)}} \right]^{\kappa_\star} \quad \text{for } \check{B}_{\rm syn(\star)}(\hat{\hat{\mathcal{D}}}) < \check{B}_{\rm syn(p)}(\hat{\hat{\mathcal{D}}}), \qquad (37b)$$

where $\hat{\hat{\mathcal{E}}}_{\nu,\star}(\hat{\hat{\mathcal{D}}})$ is given by Eq. (31c). The power law indices in Eqs. (37) are $\kappa_p = \frac{2}{7}$ and $\kappa_\star = \frac{3}{10}$ for $\Omega^* = \Omega = \rm const > \hat{\hat{\mathcal{D}}}^{-2}$, while $\kappa_p = \kappa_\star = \frac{1}{2}$ with $\Omega^* = \mathcal{D}^{*-2}$ in the case of a free jet, $\Omega \sim \mathcal{D}^{-2}$. Equations (37) are indeed true upper limits for $\hat{\mathcal{E}}_\nu$: increasing $\mathcal{D}$ beyond $\hat{\hat{\mathcal{D}}}$ while keeping $\xi_{B\gamma} = \xi_{B\gamma,\rm max}$, implies $B \propto \mathcal{D}^{-3}$ for constant Ω, and $B \propto \mathcal{D}^{-2}$ for a free jet; since the maximum energy is determined by the adiabatic limit, Eq. (14), this leads to $\hat{\mathcal{E}}_\nu \propto \mathcal{D}^{-1}$ and $\hat{\mathcal{E}}_\nu \propto \rm const$, respectively. It is obvious that any other choice of parameters, e.g., $\mathcal{D} < \hat{\hat{\mathcal{D}}}$ or $\xi_{B\gamma} < \xi_{B\gamma,\rm max}$, leads to lower limiting energies. From Eq. (35b) we obtain

$$\hat{\hat{\ell}}_\nu \leq \hat{\hat{\ell}}_{\nu,p}(\hat{\hat{\mathcal{D}}}) = \frac{\overline{\xi}_{pB}\xi^*_{B\gamma}}{4 b_p f^*_{p\gamma}} \left[\frac{4\pi\mathfrak{E}_T}{\Omega^* b_{\rm ph}\mathcal{L}_{\rm b}\mathcal{T}(1+\overline{\xi}_{pB})\xi^*_{B\gamma}} \right]^{\lambda_p} \quad \text{for } \check{B}_{\rm syn(\star)}(\hat{\hat{\mathcal{D}}}) \geq \check{B}_{\rm syn(p)}(\hat{\hat{\mathcal{D}}}) \qquad (38a)$$

$$\hat{\hat{\ell}}_\nu \leq \hat{\hat{\ell}}_{\nu,\star}(\hat{\hat{\mathcal{D}}}) = \frac{\overline{\xi}_{pB}\check{B}^*_{B\gamma,\rm syn(\star)}}{4 b_p f^*_{p\gamma}} \left[\frac{4\pi\mathfrak{E}_{\rm T}}{\Omega^* b_{\rm ph}\mathcal{L}_{\rm b}\mathcal{T}(1+\overline{\xi}_{pB})\xi^*_{B\gamma}} \right]^{\lambda_\star} \quad \text{for } \check{B}_{\rm syn(\star)}(\hat{\hat{\mathcal{D}}}) < \check{B}_{\rm syn(p)}(\hat{\hat{\mathcal{D}}}), \qquad (38b)$$

with $\lambda_p = (2-a)/7$ and $\lambda_\star = (3-a)/10$ for $\Omega = \Omega^* = \rm const$, and $\lambda_p = (2-a)/4$, $\lambda_\star = (3-a)/6$, and $\Omega^* = \mathcal{D}^{*-2}$ in the case of a free jet. Equation (33) is not an upper limit, because higher values are generally allowed for lower Doppler factors; thus, one can increase the emitted neutrino power compared to the value in Eqs. (38) on the expense of the maximum neutrino energy. We also emphasize the role of the baryonic energy content: increasing $\overline{\xi}_{pB}$ increases $\hat{\hat{\ell}}_\nu(\hat{\hat{\mathcal{D}}})$, but decreases $\hat{\hat{\mathcal{D}}}$ and therefore the upper limit on $\hat{\hat{\mathcal{E}}}_\nu$. We note that the dependence on the value of $\hat{\hat{\mathcal{D}}}$ is low, so that in many cases $\hat{\mathcal{E}}^*_\nu$ and ℓ^*_ν will give good order-of-magnitude estimates on the possible ultra-high energy neutrino of a transient. We illustrate this discussion in some more specific applications in the next section.

IV. NEUTRINO EMISSION FROM UNSTEADY ASTROPHYSICAL SOURCES

In this section, we apply the general theory developed in Sec. III to specific models of astrophysical transients, which are commonly discussed in the literature. Our aim is to explore the parameter space of these models more extensively than usually done in the literature, and to check the results for consistency with the limits set by secondary particle cooling, which is disregarded in most papers. To simplify the discussion, we ignore in the following the geometric parameters x_L and ρ_T introduced in the last section, and assume $x_L=\rho_T=1$. However, since all times are normalized by the size of the emission region, and all luminosities by the photon energy density in the comoving frame, they can easily be reintroduced by replacing $\mathcal{T}\to\mathcal{T}\rho_T$ and $\mathcal{L}\to\mathcal{L}/x_L$ in all equations of this section.

A. Neutrinos from AGN jets

There are two classes of AGN models which predict neutrino emission, both involving normal e-p flows. One class assumes particle acceleration at shocks in the accretion flow very close to the black hole, and produce neutrinos by both $p\gamma$ and pp interactions [6,8,10,37]. The other applies to radio loud AGN, which show extended radio jets, and locates the emission region at internal shocks in the relativistic jets at larger distances from from the black hole [9,10]. The highest energy neutrinos would then be expected from *blazars*, which are AGN jets pointing in the direction of the observer, because the energy is boosted by the Doppler factor $\mathcal{D}\sim\Gamma_{\rm jet}\gg 1$ [38]. We discuss this class of models, i.e., the *AGN jet models*, in the following; some interesting implications of our results on the other class, the *AGN core models*, are described in Appendix E.

1. The ''proton blazar'' scenario

Blazars are known to emit electromagnetic radiation from radio wavelengths up to the TeV-gamma ray regime. Their spectrum shows a typical ''two-hump'' structure, where characteristic photon energies depend on the source luminosity: In high luminosity blazars, such as 3C 279, the lower hump cuts off at optical wavelengths, while the high energy emission extends up to at least 10 GeV; in low luminosity sources, such as in the nearby objects Mkn 421 and Mkn 501, the lower hump extends in flares up to 10–100 keV [39,40], and the high energy emission is observed up to $\gtrsim$10 TeV [15,41]. While there is agreement that the low energy hump is due to synchrotron emission of energetic electrons, the origin of the high energy emission is unclear: It can be explained (a) by inverse-Compton emission of the same electron population producing the low energy synchrotron radiation (e.g., [17,42], and references therein), which could arise also if the jets are leptonic (consisting of $e^{\pm}$ and magnetic fields, with few or no protons), or (b) by electromagnetic cascades induced from the decay of photohadronic pions [21]. The latter mechanism is referred to as the ''proton blazar'' or simply ''hadronic'' scenario, and gives rise to considerable neutrino fluxes [9,16], while the leptonic models obviously do not. On the basis of gamma ray observations alone, the issue of the dominant radiation process in AGN jets is not settled yet [43]; the observation of correlated neutrinos could resolve this issue.

The typical bulk Lorentz factors $\Gamma_{\rm jet}$ of AGN jets can be estimated from the apparent superluminal motion of blobs in the jet; a recent investigation of 43 AGN indicates that $\Gamma_{\rm jet}\lesssim 30$ [44], and the typical inclination angle of the blazar jets to the line of sight is inferred to be $\langle\Theta_{\rm view}\rangle_{\rm bl}\sim 5°$, confirming the estimate $\mathcal{D}\sim\Gamma_{\rm jet}\sim 10$ obtained from AGN unification models [45]; we will use $\mathcal{D}\lesssim 30$ as an upper limit estimate. A lower limit on the Doppler factor of TeV blazars can be found from the observed emission of photons with $\varepsilon\sim 1$ TeV, where the emission region must be optically thin with respect to $\gamma\gamma\to e^+e^-$ reactions of gamma-rays on intrinsic soft photons, which leads to $\mathcal{D}\gtrsim 2\mathcal{L}_{\rm x,45}^{1/5}\mathcal{T}_4^{-1/5}$, or roughly $\mathcal{D}\gtrsim 3$. A similar limit is obtained for the high luminosity blazar 3C279, using EGRET observations and assuming the emission to be optically thin at 1 GeV [32].

In contrast to the bulk Lorentz factor, the magnetic field strength in blazars is more difficult to estimate, although hadronic models typically invoke $B\gtrsim 10$ G based on equipartition arguments [46]. A test of this claim is possible by observing the synchrotron-self absorption frequency of the *variable* emission of blazars; an analysis of the spectral shape and the multifrequency variability of blazars suggests that this turnover is at an observed frequency $\sim$300 GHz [47]. Boosting into the comoving frame of the blob with $\mathcal{D}\lesssim 10$, this would be consistent with synchrotron-self absorption for $B\sim 10$ G and a relativistic electron energy density $u_e\ll B^2/8\pi$, which is expected in hadronic models [16].

The emission from blazars is strongly variable, with activity periods taking turns with quiescent periods on a typical time scale of months [48]; this kind of long-term variability is observed at all frequencies, and appears to be largely correlated. Also within an activity period, the TeV emission from Mkn 421 and Mkn 501 shows clearly separated flares with doubling time scales from days down to less than one hour [41,49], viz., $\mathcal{T}\sim 10^3-10^6$ s, with correlated variability of the synchrotron emission at x-ray energies [50]. This suggests an identification of these short-term flares with transient, causally disconnected acceleration regions of energetic particles, e.g., as expected in the scenario of internal shocks in the jets.

2. The parameter space for time-integrated neutrino spectra from blazar flares

We assume that the relevant target photons for photohadronic pion production are the synchrotron photons in the low energy spectral hump produced by accelerated electrons, since the number density of photons in the high energy hump is too low and can be neglected. We confine the discussion to low luminosity TeV blazars, where the low energy photon spectrum extends to $\epsilon\gtrsim 1$ keV; for high luminosity blazars, like 3C279, in which the synchrotron component cuts off at optical frequencies, our power law approximation is not applicable and a more detailed calculation would be required. The target photon spectrum in the comoving frame of the relativistic flow can then be approximated by a power law with a typical index $\langle a\rangle\approx 1.7$, if we use a power law inter-

polation between the sub-mm and x-ray wave bands [47], ignoring the observed break at optical frequencies; this is also justified by the observation that in flares the important optical-to-x-ray spectrum of low luminosity blazars seems to be flatter than the typical $\langle a_{ox}\rangle \approx 2$ seen in the quiescent state [40,50,51]. In the following, we adopt $a=\frac{5}{3}$ and introduce the Doppler factor and magnetic field in canonical units, $\mathcal{D}_1 \equiv \mathcal{D}/10$, and $B_1 = B/10$ G. For the break energy we use $\varepsilon_b \sim 10^{-4}$ eV [47], and $\hat{\varepsilon} \sim 1-10$ keV from x-ray observations of flares in Mkn 421 and Mkn 501 [40,52], leading to $b_{ph} \sim 10^3$. The luminosity at the spectral break is not taken from observed fluxes at ε_b, because the emission at low energy is likely to be superposed by the emission from other jet regions not associated with the flare; rather, we use the observed, isotropized x-ray luminosity at $\varepsilon_x \approx 1$ keV of the flare, $\mathcal{L}_x = [10^{45}\ \text{erg/s}]\mathcal{L}_{x,45}$, and determine $\mathcal{L}_b$ from scaling with the assumed power law photon spectrum, $\mathcal{L}_b = \mathcal{L}_{x,45}(\varepsilon_b/\varepsilon_x)^{1/3}$; note that $b_{ph}\mathcal{L}_b \sim 3\mathcal{L}_x$. Opacity requirements suggest that for low luminosity TeV blazars the external radiation does not dominate over the synchrotron component in the comoving frame of the flow [53]; if this would be the case, the thermal-like properties of the disk radiation would yield a neutrino spectra substantially different from our results.

For the characteristic Lorentz factor in the comoving frame we find $\gamma_b \sim [3\times 10^{11}]\mathcal{D}$, which is of the order the maximum proton Lorentz factors observed in cosmic rays. We will show below that acceleration of protons in blazars cannot reach higher Lorentz factors, and confine ourselves to the case $\gamma_p < \gamma_b$. In order to ignore the upper limit in the photon spectrum, we have to require $\gamma_p \gtrsim 10^{6-7}\mathcal{D}_1$.

To estimate the relevant time scale for the transient emission, $\mathcal{T}$, we use the x-ray variability, where we have to consider *electron* cooling times of order [30 s] $B_1^{-3/2}\mathcal{D}_1^{-1}$ in the observer frame, which for standard parameters are much shorter than the observed rise or decay times of the flare. This suggests that one can use Eq. (13), which explains the generally longer decay times by Lorentz boosting effects in transrelativistic internal shocks, rather than by slow cooling. We note that this is in contrast to the usual interpretation of $\mathcal{T}$ as the doubling time of the flare, which assumes much longer cooling times expected in the weak magnetic fields required by purely leptonic emission models to explain $\mathcal{T}_\downarrow > \mathcal{T}_\uparrow$. The latter explanation may also apply to hadronic models, if second order Fermi acceleration plays a role, so that in principle $\mathcal{T} = \mathcal{T}_\downarrow - \mathcal{T}_\uparrow$ can only be considered as an upper limit. The typical time scales of blazar flares are then $\mathcal{T} \equiv [10^4\ \text{s}]\mathcal{T}_4$ with $0.1 \lesssim \mathcal{T}_4 \lesssim 10$, corresponding to a comoving linear size of the emission region $R_\parallel \sim [3\times 10^{15}\ \text{cm}]\mathcal{T}_4\mathcal{D}_1$. The fact that we probably have to deal with transrelativistic shocks also suggests $\theta_F \approx 1$, which we assume in numerical estimates; in general, however, we keep θ_F as a free parameter.

In a free relativistic jet we have $t_{ad} \approx T_{cr}$, i.e., the emission region expands with the velocity of light, but $\beta_{ex} < 1$ is also possible if the jets are confined. Heuristically, we can express the value of β_{ex} by the opening angle of the jet, $\beta_{ex} \approx \min(1, \Theta_{jet}\Gamma_{jet})$, and assume $\Theta_{jet} \lesssim \langle\Theta_{view}\rangle_{bl} \sim 0.1$, which means that $\Gamma_{jet} \sim 10$ corresponds to $\beta_{ex} \lesssim 1$. Hence, existing observations cannot decide whether magnetic confinement applies or not, but β_{ex} can be expected to be close to 1. On the other hand standard jet theory assumes that $B \propto R^{-1}$ [54], i.e., $\alpha = 1$, but $\alpha = 2$ may apply if reconnection isotropizes the magnetic field as assumed in gamma-ray bursts [55]. Since β_{ex} and α always appear as a product in the equation, $\alpha\beta_{ex} \approx 1$ is a reasonable assumption, and will be used in the following. The energy limit set by adiabatic cooling then corresponds to $\rho_L \approx \frac{1}{3}\theta_F^{-1}$, so that our canonical assumption $\theta_F \approx 1$ is equivalent to the assumption that particles are accelerated up to their Larmor limit.

Using these standard parameters, we find for the star-point of the parameter space

$$\mathcal{D}_1^* \approx 0.6 \times \mathcal{L}_{X,45}^{9/40}\mathcal{T}_4^{-7/40}\theta_F^{-1/10} \tag{39a}$$

$$B_1^* \approx 6 \times \mathcal{L}_{X,45}^{-3/20}\mathcal{T}_4^{-11/20}\theta_F^{2/5} \tag{39b}$$

$$\xi_{B\gamma}^* \sim 50 \times \mathcal{L}_{X,45}^{1/20}\mathcal{T}_4^{-3/20}\theta_F^{1/5}, \tag{39c}$$

corresponding to a maximum neutrino energy

$$\hat{\mathcal{E}}_\nu^* \approx 2\times 10^{18}\ \text{eV} \times \mathcal{L}_{X,45}^{3/10}\mathcal{T}_4^{1/10}\theta_F^{-4/5}. \tag{39d}$$

Figure 1 shows the different regions of dominant cooling at the maximum energies, and their associated spectral shapes, where we have scaled $\mathcal{D}_1$ and B_1 relative to the star-point values. Also shown are the positions of three observed AGN flares in the parameter space, for which we assumed the magnetic field to be in equipartition (a) with the radiation density, or (b) with the energy density of protons, $u_p = 100u_e$, corresponding to standard assumptions in hadronic blazar models, and a range of possible Doppler factors $0.3 \lesssim \mathcal{D}_1 \lesssim 3$. Comparison with the regions of dominance of muon and pion cooling corresponding to these flares shows that muon particle cooling plays a role for short flares in scenario (b), if $\mathcal{D}_1 \lesssim 1$; pion cooling is mostly unimportant for usual hadronic AGN models. In most cases, the neutrino energy is limited by Larmor radius constraints of the accelerated protons, consistent with earlier assumptions [11,16].

3. Blazar neutrino maximum energies and fluxes

Keeping the magnetic field, the Doppler factor and the proton-to-electron energy ratio in blazars as free parameters, rather than adopting common assumptions, we can apply our discussion in Sec. III D to obtain general upper limits on neutrino energies and fluxes from this class of objects. We see from Fig. 1 that, for parameters typically observed in blazar flares, that $\breve{B}_{syn(\mu)}(\mathcal{D}) < \breve{B}_{syn(p)}(\mathcal{D})$, but $\breve{B}_{syn(\pi)}(\mathcal{D}) \gtrsim \breve{B}_{syn(p)}(\mathcal{D})$ for all Doppler factors in the discussed range. Therefore, $\mathcal{E}_\nu < \hat{\breve{\mathcal{E}}}_{\nu,p}(\mathcal{D})$ applies to muon neutrinos from pion decay, and $\mathcal{E}_\nu < \hat{\breve{\mathcal{E}}}_{\nu,\mu}(\mathcal{D})$ to muon and electron neutrinos from muon decay.

To find out the relevant range for the Doppler factors, we start with energetical considerations. The usual limit applied to the power of AGN jets is the Eddington luminosity of the putative black hole in the AGN, $L_{jet} \lesssim [10^{47}\ \text{erg/s}]M_{BH,9}$,

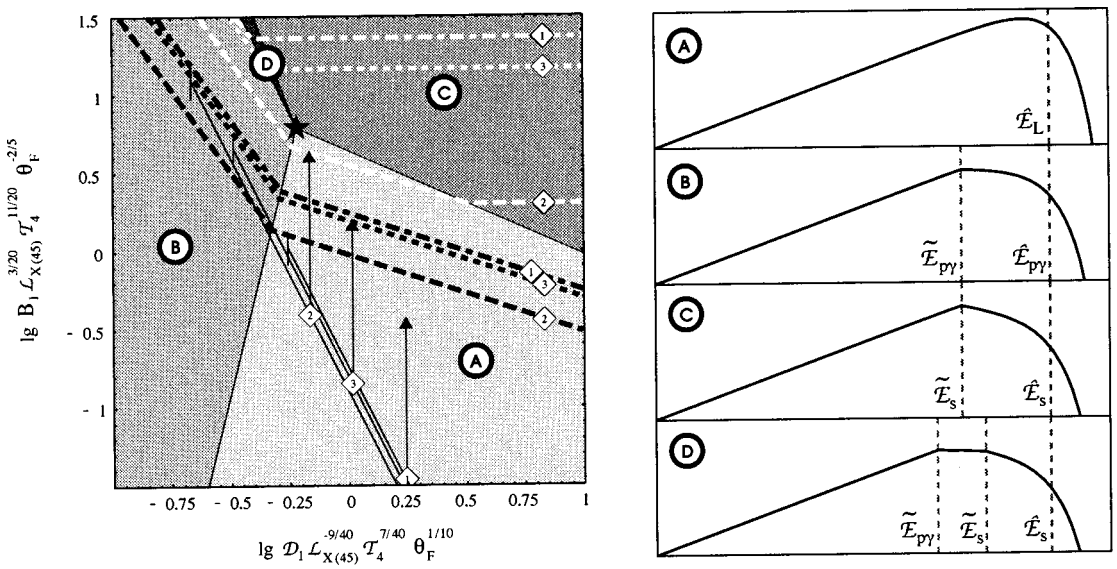

FIG. 1. Dominant cooling processes and neutrino spectral shapes for AGN jets. *Left:* Parameter space, with the ''star-point,'' denoting equal cooling time scales at the maximum energy, indicated. The shaded regions correspond to the dominant cooling process at the maximum proton energy: (A) Larmor limit or adiabatic cooling; (B) photohadronic cooling; (C) and (D) synchrotron cooling, where (D) marks the region where photohadronic cooling dominates for a part of the energy spectrum. Also shown are the positions of three observed AGN flares: ⟨1⟩ Mkn 421, April 26, 1995 ($\mathcal{T}_4=10$, $\mathcal{L}_{X,45}=0.5$) [50]; ⟨2⟩ Mkn 421, May 7, 1996 ($\mathcal{T}_4=0.1$, $\mathcal{L}_{X,45}=0.9$) [56]; ⟨3⟩ Mkn 501, April 16, 1997 ($\mathcal{T}_4=3$, $\mathcal{L}_{X,45}=2.0$) [40]. Central positions assume $u_B=u_{ph}$, black triangles correspond to $u_B=100u_{ph}$, diagonal errors indicate the range of possible Doppler factors (see text). Numbers in diamonds associate data points to the corresponding delimiting lines of muon cooling (black) and pion cooling (white); secondary particle cooling is relevant in the parameter space region above these lines. *Right:* Schematic representation of the shapes of neutrino spectra (time integrated power per logarithmic interval of energy), $\ln \mathcal{L}_\nu(\mathcal{E}_\nu)$ vs $\ln \mathcal{E}_\nu$, corresponding to regions (A)–(D). Break energies due to changes of the dominant proton cooling process are indicated (cf. Sec. II A), possible additional breaks due to secondary particle cooling are omitted for simplicity (cf. Sec. III C 2).

where $M_{BH,9}$ is the mass of the black hole in units of $10^9 M_\odot$. Since we consider a beamed emitter, we have to set $\Omega=\mathcal{D}^{-2}$. Inserting in Eq. (36), assuming an energy dissipation efficiency of $\xi_{sh}\sim 0.2$ in the jet as expected for transrelativistic internal shocks, and equipartition of proton and magnetic field energy density, $\xi_{pB}=1$, we obtain $\xi_{B\gamma,max}\sim[4\times10^3]M_{BH,9}\mathcal{L}_{X,45}^{-1}\mathcal{D}_1^2$, thus for the limiting Doppler factor allowing $\hat{\mathcal{E}}_{\nu,\pi}=\hat{\hat{\mathcal{E}}}_{\nu,\pi}$,

$$\hat{\hat{\mathcal{D}}}_{1,\pi}\approx 2\times M_{BH,9}^{3/8}\mathcal{T}_4^{-1/4}\theta_F^{-1/4}. \tag{40}$$

For the canonical range of assumed AGN black hole masses, $0.1\lesssim M_{BH,9}\lesssim 10$, we can therefore assume that $\hat{\hat{\mathcal{D}}}_\pi>\mathcal{D}^*$, for which case we find

$$\hat{\hat{\mathcal{E}}}_{\nu,\pi}(\mathcal{D}_1)\approx 4\times10^{18}\ \text{eV}\times D_1^{4/3}\mathcal{T}_4^{1/3}\theta_F^{-2/3} \lesssim 1\times10^{19}\ \text{eV}\times M_{BH,9}^{1/2}\theta_F^{-1} \tag{41a}$$

$$\hat{\hat{\nu}}_{\nu,\pi}(\mathcal{D}_1)\approx 0.3\times D_1^{2/9}\mathcal{T}_4^{-1/9}\theta_F^{2/9} \lesssim 0.3\times M_{BH,9}^{1/12}\mathcal{T}_4^{-1/6}\theta_F^{1/6}, \tag{41b}$$

where we assumed $b_p=20$. Adopting these parameters, neutrinos from muon decay are limited by muon synchrotron cooling to an energy $\hat{\mathcal{E}}_{\nu,\mu}\lesssim[8\times10^{17}\ \text{eV}]M_{BH,9}^{5/8}\mathcal{T}_4^{1/4}\theta_F^{-3/4}$. On the other hand, we can also find the conditions under which neutrinos from muon decay, in particular electron neutrinos, can reach their highest energies and fluxes. We determine $\check{\xi}^*_{B\gamma,syn(\mu)}\approx 3\mathcal{L}_{X,45}^{1/8}\mathcal{T}_4^{1/8}\theta_F^{1/2}$, leading to

$$\hat{\hat{\mathcal{D}}}_{1,\mu}\approx 5\times M_{BH,9}^{1/3}\mathcal{T}_4^{-1/3}\theta_F^{-1/3}. \tag{42}$$

Again we can confine the discussion to the case $\hat{\hat{\mathcal{D}}}_\mu>\mathcal{D}^*$, which gives

$$\hat{\hat{\mathcal{E}}}_{\nu,\mu}(\mathcal{D}_1)\approx 1\times10^{18}\ \text{eV}\times D_1^{3/2}\mathcal{T}_4^{1/2}\theta_F^{-1/2} \lesssim 1\times10^{19}\ \text{eV}\times M_{BH,9}^{1/2}\theta_F^{-1} \tag{43a}$$

$$\hat{\hat{\nu}}_{\nu,\mu}(\mathcal{D}_1)\approx 2\times10^{-2}\times D_1^{2/3}\mathcal{T}_4^{1/4}\theta_F^{3/5} \lesssim 5\times10^{-2}\times M_{BH,9}^{2/9}\theta_F^{1/3}. \tag{43b}$$

The result that the upper energy limits for neutrinos from pion and muon decay are equal in their respective optimization is a consequence of the result that the maximum energy of pion neutrinos for Doppler factors $\mathcal{D}>\hat{\hat{\mathcal{D}}}_\pi$ remains unchanged at the value $\hat{\hat{\mathcal{E}}}_{\nu,\pi}$, as discussed in Sec. III D 2. For the assumed range of AGN black hole masses and $\theta_F\gtrsim 1$, we therefore obtain a *strict* upper limit of about 3×10^{19} eV for neutrinos from AGN flares which is independent of the flare time scale and any model assumptions. The inverse linear dependence on θ_F, however, shows that this energy limit would strongly increase if we assume acceleration on time scales much shorter than the particles Larmor motion.

If the TeV emission from blazars, which has generally a luminosity comparable to the x-ray emission, ought to be explained by hadronic emission, the corresponding neutrino luminosities would have to be of the same order, or $\hat{\mathcal{L}}_\nu \sim \frac{1}{3}$. Equations (43) show that this is incompatible with the conditions neutrinos from muon decay (electron neutrinos) need to reach their theoretical energy limit of $\sim 10^{19}$ eV. For muon neutrinos from pion decay, however, this seems to be possible for very large baryonic and magnetic energy densities, $\xi_{B\gamma} \sim 10^3$; this scenario would expect a difference between the electron and muon neutrino cutoff energies of more than one order of magnitude. It should be noted, however, that proton blazars can produce $\bar{\mathcal{L}}_\nu(\hat{\mathcal{E}}_\nu) \gtrsim \mathcal{L}_X$ also for relatively moderate values of $\xi_{B\gamma}$, if $\mathcal{D} \approx \mathcal{D}^*$; then the hadronic radiative efficiency (neutrinos+gamma rays) increases to $\gtrsim 50\%$, so that a comparable emission in neutrinos, high energy and low energy photons can be achieved for $\xi_{pB} \sim \xi_{B\gamma} \sim 1$. This more realistic scenario leads to maximum neutrino energies much below the upper limits stated in Eqs. (41a) and (43a), so that flares from AGN jets would not be expected to emit considerable neutrino fluxes above a few times 10^{18} eV.

To get an estimate on event rates in current or planned VHE-UHE neutrino observatories, we consider the example of the May 7, 1997 flare of Mkn 501, which lasted 3×10^4 s. The total isotropized energy emitted in optical to x-ray photons of this flare is $\bar{\mathcal{L}}_{ox} \sim 2\times 10^{50}$ erg; taking the luminosity distance of ≈ 160 Mpc, and assuming $\bar{\mathcal{L}}_\nu \sim \bar{\mathcal{L}}_{ox}$ as suggested by TeV observations, this corresponds to a total energy in neutrinos of $\hat{\mathcal{E}}_\nu \sim 10^{18}$ eV at earth of about 6×10^5 erg km^{-2}, which would produce $\sim 3\times 10^{-7}$ neutrino induced showers per km^3 air volume. The biggest air fluorescence detectors currently planned would cover about 3×10^5 km^3 air, and the ground array of the Pierre Auger Observatory would correspond to about 5×10^3 km^3, which would clearly be not sufficient to detect the neutrino emission, of a single AGN flare. Following an $\mathcal{E}_\nu^{2/3}$ power spectrum, the total energy in neutrinos at $\mathcal{E}_\nu \sim 10^{15}$ eV would be about 6×10^3 erg km^{-2}, which would cause $\sim 3\times 10^{-3}$ events in a 1 km^3 underwater/ice Cherenkov detector. Also here, even the biggest neutrino telescope currently considered would not be able to ''see'' single AGN flares. The best we can expect is therefore to collect diffuse fluxes corresponding to many AGN flares and determine the average properties of their neutrino spectra. Details of the time integrated emission spectra of AGN correlated transients, however, would still be important to determine reliable estimates for such diffuse fluxes.

B. Gamma-ray bursts

Gamma-ray bursts (GRBs) are thought to be produced in highly relativistic outflows originating from a compact, explosive event over time scales of less than a second up to several minutes [57,58]. Recent observations of GRB afterglows [59] indicate that they are located at cosmological distances, which requires a characteristic luminosity of about $\gtrsim 10^{51}$ erg s^{-1} under the assumption of isotropic emission. Possible scenarios which could release that much energy over the time scales observed are, e.g., the coalescence of a neutron star binary, or the collapse of a supermassive star. The radiation observed from GRBs is expected to be due mainly to synchrotron or inverse Compton radiation from relativistic electrons accelerated at shock fronts occurring near the interface of the expanding relativistic shell (*external shocks*), or at shocks forming within the unsteady outflow itself (*internal shocks*) [60]. The same mechanisms would also accelerate protons, which could reach energies of the order of the highest energy cosmic rays, $\sim 10^{20}$ eV [61,62]. Because of the interaction with the dense photon field in the burst, these protons can produce efficiently VHE, and maybe also UHE neutrinos [14]. Neutrinos of lower energy may also be produced by *pp* interactions between cold protons in the colliding ejecta [13]. Obviously, both scenarios fall into the class of transient emission, and we can apply our results from Sec. III to examine in more detail the spectrum and maximum energy of the neutrinos from $p\gamma$ interactions in gamma-ray bursts. We note, however, that our discussion assumes that the physical parameters in the transient remain approximately constant over the emission time scale; it does therefore not apply to GRB afterglows, in which the parameters change drastically over very long time scales.

1. Cosmological fireball models and internal shocks

Many GRBs show intrinsic variability on time scales $\mathcal{T} \sim 1$ ms–1 s, while the total burst durations are typically $\mathcal{T}_{GRB} \sim 0.1$–100 s [57]. This implies that their energy is released in a volume of the typical dimension of compact or stellar objects, $R_0 \sim 10^7$–10^{10} cm. For a total energy of $\gtrsim 10^{52}$ erg, this leads to a local photon density of $\gtrsim 10^{21}$ erg cm^{-3} with photon energies $\gg m_e c^2$. These ''fireballs'' (and even much weaker ones as well) would be optically thick to $\gamma\gamma$ pair creation, and for small baryonic loads, $M_{bar} \gtrsim 10^{-6} M_\odot$, the expansion leads to a conversion of almost all the radiation energy into bulk kinetic energy of motion, accelerating to a limiting Lorentz factor of $\Gamma \sim \eta = \mathfrak{E}_{GRB}/M_{bar}c^2 \gg 1$, before photons can escape [63]. Hence, a dissipation mechanism reconverting the bulk kinetic motion into radiation is required after the flow becomes optically thin: this can be achieved by electron acceleration at shock waves occurring when the ejecta run into external matter [63]. Moreover, internal shocks can form in the ejected wind if the outflow is non-steady, i.e., η varies significantly over time scales $\ll \mathcal{T}_{GRB}$, which can lead to faster shells catching up with slower shells [24], similarly to what was discussed for AGN in Sec. III A. Such internal shocks can dissipate the kinetic energy with an efficiency comparable to external shocks. While external shocks are expected to produce a relatively featureless outburst over time scales comparable to the total burst duration, $\mathcal{T}_{GRB}$, internal shocks could be associated with the rapid variability within the burst on time scales $\mathcal{T} \ll \mathcal{T}_{GRB}$. In both external and internal shocks a substantial fraction of the gamma radiation is produced by synchrotron cooling of the shock-accelerated electrons. At the dissipation radius where internal shocks occur [24],

$$r_d \sim c\mathcal{T}\eta^2, \tag{44}$$

i.e., where the radiated gamma rays are produced, the comoving magnetic field energy density can be parametrized through $u_B = \xi_{B\gamma} u_{\rm ph}$, so that

$$B \sim 10^{10}\ {\rm G} \times (\xi_{B\gamma} b_{\rm ph} \mathcal{L}_{51})^{1/2} \mathcal{T}_0^{-1} \eta^{-3}, \tag{45}$$

where $\mathcal{T}_0 = \mathcal{T}/1$ s and $\mathcal{L}_{51} = \mathcal{L}/10^{51}$ erg s^{-1} are the normalized GRB variability time scale and isotropic luminosity at the break energy in the observer frame, respectively, and $b_{\rm ph}$ is the bolometric correction factor correlating this specific luminosity to the total gamma-ray luminosity of the burst. The value of $b_{\rm ph}$ depends essentially on the high energy cutoff in the photon emission, which cannot be inferred from current data; for internal shocks one expects $\hat{\epsilon} \lesssim 100$ MeV in the comoving frame, corresponding to a canonical value $b_{\rm ph} \approx 10$. In the internal shock model, constraints on the bulk Lorentz factor can be inferred from the requirement that the dissipation radius is larger than the radius of the photosphere, $r_{\rm ph} \sim [10^{18}\ {\rm cm}] \mathcal{L}_{51} \eta^{-3}$, below which the wind is optically thick, and the radius of the external termination shock, $r_{\rm xsh} \sim [10^{18}\ {\rm cm}] \mathcal{L}_{51}^{1/3} \mathcal{T}_{0,\rm GRB}^{1/3} \eta^{-2/3}$, which requires the bulk Lorentz factor of the ejecta, $\Gamma \sim \eta$, to be in the range $30 \lesssim \Gamma \lesssim 10^3$, leading to magnetic fields in the range $10^7\ {\rm G} \gtrsim B \gtrsim 1\ {\rm G}$, assuming equipartition between magnetic field and photons, standard values for $\mathcal{L}_{\rm b}$ and $b_{\rm ph}$, and typical time scales of 0.1 s for short-term variability, and 30 s for the total duration of a featureless burst. The latter values, $\Gamma \sim 10^3$ and $B \sim 1$ G, would imply that the internal shocks occur on similar time scales and physical conditions as the external shock, making both scenarios virtually identical with respect to the discussion of transients. Typical parameters for assumed internal shocks with $\mathcal{T} \ll \mathcal{T}_{\rm GRB}$ are $\Gamma \sim 300$ and $B \gtrsim 10^3$ G, which are also required by models predicting the acceleration of UHECR protons in this scenario [61,64].

We still need to relate the parameters R, x_L and $\mathcal{D}$, defined in Sec. III B for a causally connected emission region moving at some angle $\Theta_{\rm view}$ to the line of sight, to the parameters describing the expanding flow in a GRB. In the comoving frame of the wind (at an arbitrary point), the apparent thickness of the wind zone extending to a radius r is r/Γ. Similarly, the transversal extent of causally connected regions in the comoving frame of the flow is r/Γ, because regions farther apart move away from each other with velocities larger than c (r/Γ may thus be interpreted as the ''Hubble radius'' of the expanding emission region, cf. [63]). If the energy dissipation takes place at a radius $r_{\rm d}$ where the bulk Lorentz factor is saturated, $\Gamma \sim \eta$, the comoving ''linear size'' of the emission region can thus be written as $R \sim r_{\rm d}/\eta$. On the other hand, the isotropic luminosity of the burst in the observer frame is related to the photon energy density in the comoving frame of the wind by $\mathcal{L} = 4\pi r_{\rm d}^2 c \Gamma^2 u_{\rm ph}$, which is identical to Eq. (12) in conjunction with the linear boosting formula, $\mathcal{L} = L\mathcal{D}^4$, if we use the parameters $R = r_{\rm d}/\Gamma$, $x_L = 1$ and $\mathcal{D} = \Gamma$. For $\Gamma \sim \eta = {\rm const}$, all parameters are therefore correctly derived if we treat the GRB as emission from a spherical region of radius $R \sim r_{\rm d}/\eta$ boosted with a Doppler factor $\mathcal{D} \sim \eta$. Moreover, if the gamma ray emission originates from synchrotron radiation of electrons whose cooling time scale is much shorter than the crossing time [24], we can also apply $R \approx c\mathcal{T}\mathcal{D}$, or $\rho_T \approx 1$; since we can apply our discussion to both internal spikes in strongly variable bursts and to featureless bursts in total, we allow the value of the normalized time scale in the broad range $10^{-3} < \mathcal{T}_0 < 100$. According to our definition of the radius R as the ''Hubble radius'' of the expanding emission region, we obviously also have $\beta_{\rm ex} = 1$, and the effective space fraction available for the gyration of protons is essentially constrained by adiabatic losses, $\rho_L \sim (\pi \alpha \theta_F)^{-1}$, where both $\alpha = 1$ and $\alpha = 2$ have to be considered possible values, depending on whether the magnetic field is largely transversal or isotropized by reconnection [55].

2. GRB neutrino spectrum and maximum energy

The observed electromagnetic spectrum of a GRB can be approximately described as a broken power law, with a break energy $\varepsilon_{\rm b,GRB} \sim 300$ keV in the observer frame. The photon number spectrum is then given by $N(\epsilon) \propto \epsilon^{-2}$ for $\epsilon > \epsilon_{\rm b,GRB}$ (thus $a = 2$), and for $\epsilon < \epsilon_{\rm b,GRB}$ it is $N(\epsilon) \propto \epsilon^{-2/3}$, with $\epsilon_{\rm b,GRB} = \varepsilon_{\rm b,GRB} \mathcal{D}^{-1}$. This yields a proton break Lorentz factor in the range $10^4 \lesssim \gamma_{\rm b} \lesssim 5 \times 10^5$, corresponding to the range of possible Doppler factors given above. When we consider neutrinos of energy $\mathcal{E}_\nu \gtrsim 100$ TeV, we require proton Lorentz factors of $\gamma_p \gtrsim 3 \times 10^6/\mathcal{D}$. For $\mathcal{D} \sim 100$, we therefore have $\gamma_p \gtrsim \gamma_{\rm b}$; for simplicity, we restrict our considerations to the case $\gamma_p \gg \gamma_{\rm b}$, noting that this might be only marginally correct for the lower energy bound of the VHE neutrino regime. In a $\epsilon^{-2/3}$ low energy spectrum, we simply have $N_{\rm ph}/N_{\rm ph,b} = 4 - 3(\gamma_{\rm b}/\gamma_p)^{1/3}$ for $\gamma_p > \gamma_{\rm b}$; for simplicity, we use $N_{\rm ph}/N_{\rm ph,b} \approx 3$ for all γ_p. Introducing normalized quantities also for the Doppler factor, $\mathcal{D} = 100\mathcal{D}_2$, the magnetic field, $B = [10^3\ {\rm G}] B_3$, and the bolometric correction factor, $b_{\rm ph} = 10 b_1$, the coordinates of the star-point of the parameter space, where all proton cooling processes have equal time scales at the maximum proton energy, are then

$$\mathcal{D}_2^* \approx 0.9 \times \mathcal{L}_{51}^{1/4} \mathcal{T}_0^{-1/4} \alpha^{-1/4} \tag{46a}$$

$$B_3^* \approx 4.5 \times \mathcal{L}_{51}^{-1/6} \mathcal{T}_0^{-1/2} \theta_{\rm F}^{1/3} \alpha^{5/6} \tag{46b}$$

$$\xi_{B\gamma}^* \approx 2 \times 10^{-2} \times \mathcal{L}_{51}^{1/6} \mathcal{T}_0^{-1/2} \theta_{\rm F}^{2/3} \alpha^{1/6} b_1^{-1}. \tag{46c}$$

In the following we express the magnetic field by its equipartition parameter. Figure 2 shows the GRB parameter space and the separate regions of dominance of the various cooling processes limiting the neutrino energy, and the corresponding neutrino spectral shapes for a set of possible parameters, including both millisecond flares in internal shocks and featureless GRBs; unlike in the AGN case, we do not use parameters scaled relative to the star-point, and put more emphasis on secondary particle cooling, which we consider separately for pions and muons. We see that in all cases, the energy of neutrinos from both pion and muon decay is limited by secondary particle cooling, where synchrotron cooling of pions and muons plays the most important role. Only in a limited part of the parameter space does an additional break due to adiabatic cooling of muons appear in the spectrum, while adiabatic cooling is generally unimportant for

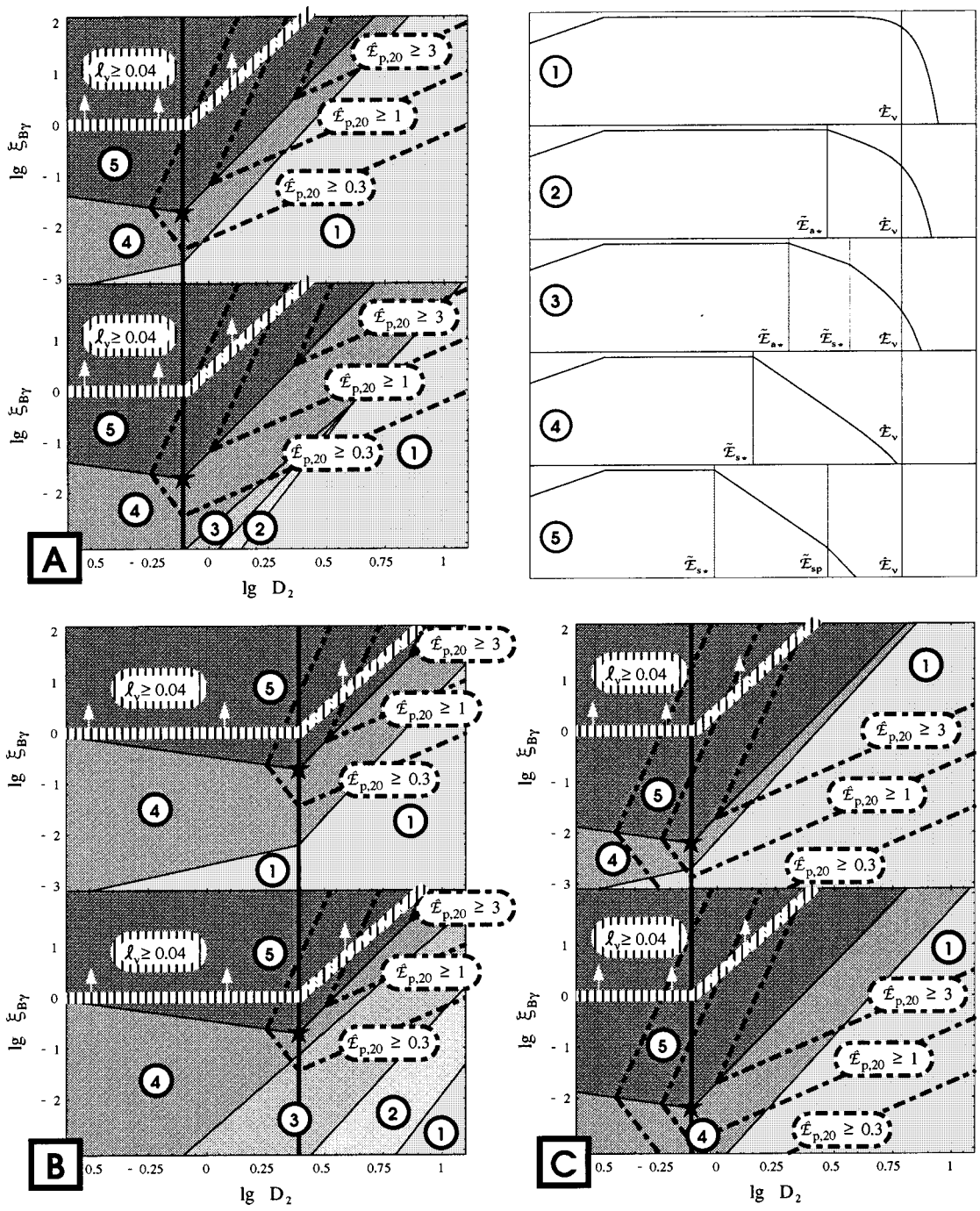

FIG. 2. Dominant cooling processes and spectral shapes for neutrino production in gamma-ray bursts. *Upper left and lower panel:* Parameter space for three different parameter sets, all assuming $\theta_F=b_1=1$, and $\alpha=2$: (A) canonical case, $\mathcal{L}_{51}=\mathcal{T}_0=1$; (B) short intrinsic flares, $\mathcal{T}=10$ ms, and $\mathcal{L}_{51}=1$; (C) extreme case for bright afterglow burst, $\mathcal{L}=3\times10^{52}$ erg s^{-1} and $\mathcal{T}=30$ s (which implies an isotropic bolometric photon energy $b_{\rm ph}\mathcal{L}_b\mathcal{T}=10^{55}$ erg, requiring $\Omega_{4\pi}\ll1$). The central line divides regions where photohadronic cooling dominates adiabatic cooling (left from the line), and vice versa (right from the line), the star-point of equal proton cooling times at the maximum energy is indicated. Shaded regions correspond to spectral shapes produced by the subsequent change of dominant proton and secondary particle cooling processes: (1) adiabatic/photohadronic cooling dominant up to $\hat{\mathcal{E}}_\nu$; (2) $\tilde{\mathcal{E}}_{\nu,\mathrm{ad}(\star)}<\hat{\mathcal{E}}_\nu$; (3) $\tilde{\mathcal{E}}_{\nu,\mathrm{ad}(\star)}<\tilde{\mathcal{E}}_{\nu,\mathrm{syn}(\star)}<\hat{\mathcal{E}}_\nu$; (4) $\tilde{\mathcal{E}}_{\nu,\mathrm{syn}(\star)}<\hat{\mathcal{E}}_\nu$; (5) $\tilde{\mathcal{E}}_{\nu,\mathrm{syn}(\star)}<\tilde{\mathcal{E}}_{\mathrm{syn}(p)}<\hat{\mathcal{E}}_\nu$. In each figure, the upper part corresponds to neutrinos from pion decay and the lower part for neutrinos from muon decay. Also indicated are the regions allowing UHE cosmic ray production up to $\hat{\mathcal{E}}_{p,20}$ (black chain lines), and the region corresponding to the neutrino fluxes predicted in Ref. [14], for $\xi_{pB}=1$ (white hatched line and arrows). *Upper right:* Schematic representation of corresponding spectral shapes, log $\mathcal{L}_\nu(\mathcal{E}_\nu)$ vs log $\mathcal{E}_\nu$, corresponding to regions (1)–(5). The lower break indicates the spectral change at about 100 TeV due to the change of the photon target spectrum at $\gamma_p\sim\gamma_b$ (see Ref. [14]), which is not discussed in this paper.

pions. At the star-point, the maximum neutrino energy from gamma-ray bursts is therefore considerably below $\hat{\mathcal{E}}_\nu^*$, so that we omit its value here to avoid confusion.

Because of the dominance of secondary particle cooling, Eqs. (31) must be used to determine the neutrino energy limit at a given Doppler factor, $\hat{\hat{\mathcal{E}}}_\nu(\mathcal{D})$, which is reached along a line $\xi_{B\gamma}=\check{\xi}^*_{B\gamma,\mathrm{syn}(\star)}(\mathcal{D}/\mathcal{D}^*)^5$ in the parameter space, with

$$\check{\xi}^*_{B\gamma,\mathrm{syn}(\pi)}=2.3\times10^{-4}\times\mathcal{L}_{51}^{1/4}\theta_\mathrm{F}\mathcal{T}_0^{-1/4}\alpha^{-1/4}b_1^{-1} \tag{47a}$$

$$\check{\xi}^*_{B\gamma,\mathrm{syn}(\mu)}=1.7\times10^{-5}\times\mathcal{L}_{51}^{1/4}\theta_\mathrm{F}\mathcal{T}_0^{-1/4}\alpha^{-1/4}b_1^{-1}. \tag{47b}$$

Recent observations of GRB afterglows at large redshifts require a total isotropic energy emitted in photons of $b_\mathrm{ph}\mathcal{L}_\mathrm{b}\mathcal{T}_\mathrm{GRB}\gtrsim10^{53}$ erg [59]. Since this value comes very close to the gravitational energy released in the collapse of a compact object (e.g., a neutron star), it is most likely that the energy of a GRB is not emitted isotropically. Moreover, efficient hadronic emission of GRB has to assume that comparable amounts of energy are present also in other channels, like magnetic fields or protons. While collimation into jets is a distinct possibility, the evidence for it is not as obvious as in AGN; in the following we assume that the GRB energy is emitted into a ''firecone'' of solid angle $4\pi\gg\Omega\gg\mathcal{D}^{-2}$, and we introduce the normalized solid angle $\Omega_{4\pi}\equiv\Omega/4\pi\ll1$. For GRB with a strongly variable light curve, the transients considered here are single, isolated radiation spikes rather than the whole burst; if we assume, however, that the total energy is equally distributed over the individual flares and that there are no extended gaps in the light curve, we have $\mathfrak{E}_T/b_\mathrm{ph}\mathcal{L}_\mathrm{b}\mathcal{T}\sim\mathfrak{E}_\mathrm{GRB}/b_\mathrm{ph}\mathcal{L}_\mathrm{b}\mathcal{T}_\mathrm{GRB}$, which again allows a common description of both subflares within GRB and featureless bursts. For simplicity, we assume in the following parameters which allow relativistic protons and magnetic fields to dominate the energy, $\underline{\xi_{pB}}\sim1$ and $\xi_{B\gamma,\max}\sim\Omega_{4\pi}^{-1}\mathcal{L}_{51}^{-1}\gg1$, and neglect the dependency on the weakly varying factors α and b_1, leading to

$$\hat{\hat{\mathcal{D}}}_{2,\pi}\approx5\times\Omega_{4\pi}^{-1/5}\mathcal{T}_0^{-1/5}\theta_\mathrm{F}^{-1/5} \tag{48a}$$

$$\hat{\hat{\mathcal{D}}}_{2,\mu}\approx8\times\Omega_{4\pi}^{-1/5}\mathcal{T}_0^{-1/5}\theta_\mathrm{F}^{-1/5}, \tag{48b}$$

which means that we only need to discuss the case $\hat{\hat{D}}_\mu>\mathcal{D}^*$. We then obtain for the neutrino energy limit

$$\begin{aligned}\hat{\hat{\mathcal{E}}}_{\nu,\pi}(\mathcal{D}_1)&\approx1\times10^{18}\ \mathrm{eV}\times D_2^{3/2}\mathcal{T}_0^{1/2}\theta_\mathrm{F}^{-1/2}\\&<1\times10^{19}\ \mathrm{eV}\times\Omega_{4\pi}^{-3/10}\mathcal{T}_0^{1/5}\theta_\mathrm{F}^{-4/5}\end{aligned} \tag{49a}$$

$$\begin{aligned}\hat{\hat{\mathcal{E}}}_{\nu,\mu}(\mathcal{D}_1)&\approx4\times10^{17}\ \mathrm{eV}\times D_2^{3/2}\mathcal{T}_0^{1/2}\theta_\mathrm{F}^{-1/2}\\&<1\times10^{19}\ \mathrm{eV}\times\Omega_{4\pi}^{-3/10}\mathcal{T}_0^{1/5}\theta_\mathrm{F}^{-4/5}.\end{aligned} \tag{49b}$$

It therefore seems that photohadronic neutrinos from GRBs can reach energies up to 10^{19} eV and above. However, the corresponding normalized neutrino luminosities at the neutrino energy limit are

$$\begin{aligned}\hat{\hat{\ell}}_{\nu,\pi}(\mathcal{D}_2)&\approx2\times10^{-6}\times D_2\theta_\mathrm{F}\\&<1\times10^{-5}\times\Omega_{4\pi}^{1/5}\mathcal{T}_0^{-1/5}\theta_\mathrm{F}^{4/5}\end{aligned} \tag{50a}$$

$$\begin{aligned}\hat{\hat{\ell}}_{\nu,\mu}(\mathcal{D}_2)&\approx2\times10^{-7}\times D_2\theta_\mathrm{F}\\&<1\times10^{-6}\times\Omega_{4\pi}^{1/5}\mathcal{T}_0^{-1/5}\theta_\mathrm{F}^{4/5},\end{aligned} \tag{50b}$$

which shows that even in the limiting case $\mathcal{D}=\hat{\hat{\mathcal{D}}}$ only very small fractions of the photon energy can be emitted in neutrinos at the limiting energy. Since we assumed $\underline{\xi_{pB}}\sim1$ and $\xi_{B\gamma,\max}\gtrsim1$ in our calculations, the low values of $\hat{\hat{\ell}}_\nu$ are clearly due to a very low efficiency along the line $\xi_{B\gamma}=\check{\xi}_{B\gamma,\mathrm{syn}(\star)}(\mathcal{D})$. Assuming a neutrino conversion efficiency of $\zeta_\nu\sim0.2$, $\xi_{B\gamma}\sim1$ and $u_p\sim5\epsilon_\mathrm{b}^2(dN_\mathrm{ph}/d\epsilon)_{\underline{\mathrm{b}}}$, which is consistent with our equipartition assumption, $\underline{\xi_{pB}}\sim\xi_{B\gamma}\sim1$, for $b_\mathrm{ph}\sim b_p\approx5$, viz., $\ell_\nu\sim0.04$, Waxman and Bahcall [14] derived a GRB-related neutrino event rate at $\mathcal{E}_\nu\gtrsim10^{14}$ eV of about 10–100 per year in a km^3 detector. This event rate would be below the expected background, but still statistically significant because of the time and directional correlation to the bursts. It is clear from the above that if we try to maximize the neutrino energy in the UHE range, following Eq. (49), this estimate would have to be reduced by more than 4 orders of magnitude, leading to insignificant event rates at these highest energies even if the usually larger detector volume of UHE experiments is taken into account.

We can also turn the question around and ask which is the region of parameter space where neutrino fluxes of the magnitude predicted by Waxman and Bahcall [14] are expected, i.e., $\ell_\nu\gtrsim0.04$, and then derive the maximum neutrino energy for these parameters. The assumptions of Waxman and Bahcall for a single burst (or subflare) can be essentially put in the form $\underline{\mathcal{L}_\nu\sim0.2\mathcal{L}_\mathrm{b}\mathcal{T}_,}$ which can be rewritten in the form of Eq. (33) as $b_\mathrm{ph}\zeta_\nu\xi_{B\gamma}\underline{\xi_{pB}}\gtrsim0.2b_p$. To optimize the efficiency, we have to evaluate ζ_ν at an energy where it is not yet diminished by synchrotron cooling of either protons or secondary particles; since $\mathcal{D}>\mathcal{D}^*$, this means that we have to use Eq. (32b) for $a=1$. For $b_p\sim b_\mathrm{ph}$ and $\underline{\xi_{pB}}\sim1$ this leads to the condition $\xi_{B\gamma}\gtrsim(\mathcal{D}/\mathcal{D}^*)^4$ for $\mathcal{D}\gtrsim\mathcal{D}^*$; for $\mathcal{D}<\mathcal{D}^*$, the efficiency is constant since photohadronic cooling dominates. Figure 2 shows that this region of the parameter space is entirely enclosed by the regions of pion, muon and proton synchrotron cooling dominance, which means that $\tilde{\mathcal{E}}_{\nu,\mathrm{syn}(\star)}$ has to be used as the maximum neutrino energy, according to our assumption of adiabatic cooling dominance. Inserting into Eq. (20) we obtain

$$\begin{aligned}\hat{\mathcal{E}}_{\nu,\pi}&<7\times10^{16}\ \mathrm{eV}\times\mathcal{D}_2^2\mathcal{T}_0^{1/2}\\&<6\times10^{16}\ \mathrm{eV}\times\Omega_{4\pi}^{-1/2}\end{aligned} \tag{51a}$$

$$\begin{aligned}\hat{\mathcal{E}}_{\nu,\mu}&<5\times10^{15}\ \mathrm{eV}\times\mathcal{D}_2^2\mathcal{T}_0^{1/2}\\&<4\times10^{15}\ \mathrm{eV}\times\Omega_{4\pi}^{-1/2},\end{aligned} \tag{51b}$$

where the second limit was derived using $\xi_{B\gamma}<\Omega_{4\pi}^{-1}\mathcal{L}_{51}^{-1}$ and $\Omega_{4\pi}\ll 1$. This means that gamma-ray bursts can still produce UHE neutrinos with considerable fluxes, but probably not above 10^{18} eV.

While this paper was in preparation, it has been proposed by Vietri [65] that neutrinos of more than 10^{19} eV can be produced in external shocks of GRB and in GRB afterglows, with fluxes observable in very large scale air shower experiments. Concerning the external shock of the main burst, this prediction is clearly in conflict with our upper limit stated in Eqs. (50a)–(51b). In the afterglow, the larger time scales and lower photon energies make the situation rather comparable to blazar jets, and Eqs. (51) do not apply; on the basis of the considerations presented here, we cannot rule out the possibility of producing neutrinos of such extreme energies in afterglows. It has been recently shown that such large UHE neutrino fluxes would also be in conflict with the assumption that (a) the cosmic ray production spectrum is $\propto\gamma_p^{-2}$, as assumed also here, and (b) that the locally observed cosmic ray energy density above 10^{19} eV is homogeneous throughout the universe and does not evolve with cosmological redshift [66].

3. The relation between cosmic ray and neutrino maximum energies

GRBs have been proposed as possible sources for the highest energy cosmic rays [61,62], which are observed up to $\hat{\mathcal{E}}_p\sim 3\times 10^{20}$ eV [19]. The maximum proton energy in the observer frame is $\hat{\mathcal{E}}_p=m_pc^2\hat{\gamma}_p\mathcal{D}$; at the star-point of the parameter space, we find $\hat{\mathcal{E}}_p^{\star}\approx[1\times 10^{20}\ \mathrm{eV}]\mathcal{L}_{51}^{1/3}\theta_{\mathrm{F}}^{-2/3}\alpha^{-2/3}$. The highest proton energy for a given Doppler factor is obviously achieved at the line of equal time scales for proton synchrotron cooling and adiabatic losses (the same condition which determines the maximum neutrino energy if secondary particle cooling plays no role). This is the border line of region (5) in the parameter space shown in Fig. 2, so we find $\hat{\mathcal{E}}_p=\hat{\mathcal{E}}_p^{\star}(\mathcal{D}/\mathcal{D}^*)^{4/3}$ for $\mathcal{D}\gtrsim\mathcal{D}^*$, leading to

$$\hat{\check{\mathcal{E}}}_p(\mathcal{D}_2)\approx 1\times 10^{20}\ \mathrm{eV}\times\mathcal{D}_2^{4/3}\mathcal{T}_0^{1/3}\theta_{\mathrm{F}}^{-2/3}\alpha^{-1/3}. \tag{52}$$

Since $\xi_{B\gamma}\propto\mathcal{D}^{14/3}$ along this line, the required magnetic field equipartition parameter rises fast; as a function of the proton energy in the observers frame, $\hat{\mathcal{E}}_{p,20}$, in units of 10^{20} eV, we can formulate the minimum requirements in $\mathcal{D}$ and $\xi_{B\gamma}$ as

$$\check{\mathcal{D}}_{\mathrm{UHE}}(\hat{\mathcal{E}}_{p,20})\approx 90\times\hat{\mathcal{E}}_{p,20}^{3/4}\mathcal{T}_0^{-1/4}\theta_{\mathrm{F}}^{1/2}\alpha^{1/4} \tag{53a}$$

$$\check{\xi}_{B\gamma,\mathrm{UHE}}(\hat{\mathcal{E}}_{p,20})\approx 0.01\times\hat{\mathcal{E}}_{p,20}^{7/2}\mathcal{T}_0^{-1/2}\theta_{\mathrm{F}}^{3}\alpha^{5/2}\mathcal{L}_{51}^{-1}b_1^{-1}. \tag{53b}$$

In correspondence with the result of Waxman [61], we find that bulk Lorentz factors $\mathcal{D}\gtrsim 300$ and magnetic fields close to equipartition with the radiation ($\xi_{B\gamma}\sim 1$) are sufficient to produce the highest energy cosmic rays, $\hat{\mathcal{E}}_{p,20}\gtrsim 3$, provided that protons are accelerated on their Larmor time scale. Assuming minimal conditions for the production of UHE cosmic rays, i.e., $\mathcal{D}=\check{\mathcal{D}}_{\mathrm{UHE}}(\hat{\mathcal{E}}_{p,20})$ and $\xi_{B\gamma}=\check{\xi}_{B\gamma,\mathrm{UHE}}(\hat{\mathcal{E}}_{p,20})$, we can derive the corresponding maximum neutrino energy as a function of $\hat{\mathcal{E}}_{p,20}$ as

$$\hat{\mathcal{E}}_{\nu,\pi}\big|_{\hat{\mathcal{E}}_p=\hat{\check{\mathcal{E}}}_p(\mathcal{D})}\sim 5\times 10^{17}\ \mathrm{eV}\times\hat{\mathcal{E}}_{p,20}^{5/4}\theta_{\mathrm{F}}^{1/2}\mathcal{T}_0^{1/4}\alpha^{-1/4} \tag{54a}$$

$$\hat{\mathcal{E}}_{\nu,\mu}\big|_{\hat{\mathcal{E}}_p=\hat{\check{\mathcal{E}}}_p(\mathcal{D})}\sim 3\times 10^{16}\ \mathrm{eV}\times\hat{\mathcal{E}}_{p,20}^{5/4}\theta_{\mathrm{F}}^{1/2}\mathcal{T}_0^{1/4}\alpha^{-1/4} \tag{54b}$$

where we again assume $\hat{\mathcal{E}}_{\nu,\star}=\hat{\mathcal{E}}_{\nu,\mathrm{syn}(\star)}$. We see that, although secondary particle cooling limits the neutrino energies to values much below the canonical $\hat{\mathcal{E}}_\nu=0.05\hat{\mathcal{E}}_p$ assumption, the maximum neutrino energy still has a tendency to increase with $\hat{\mathcal{E}}_p$. However, Eqs. (54) assume just minimal conditions for the production of UHE cosmic rays, while the region of the parameter space corresponding to $\hat{\mathcal{E}}_p\gtrsim[10^{20}\ \mathrm{eV}]\hat{\mathcal{E}}_{p,20}$, as shown in Fig. 2, allows neutrino break energies principally somewhat above or below the value stated in Eqs. (54) for given $\hat{\mathcal{E}}_{p,20}$.

We note, however, that according to the standard assumptions of shock acceleration, neutrino production and cosmic ray ejection from magnetically confined sources are physically connected processes. Although it is a distinct possibility that cosmic ray acceleration to $\hat{\mathcal{E}}_p>10^{20}$ eV on the one hand, and efficient VHE neutrino production requiring only cosmic rays of lower energy on the other, may happen at different radii in the expanding shell [66], the *ejection* of UHE cosmic rays is nontrivial in this scenario, since the particles are advected downstream, and thus accumulate inside the expanding shell and remain magnetically confined. As the shell continues to expand and the comoving magnetic field decreases, the cosmic rays would lose most of their energy by adiabatic cooling, before they eventually escape when the shock slows down. The easiest way to circumvent this problem, and to eject cosmic rays with the high energies they receive at the shock, is to convert them into neutrons in, e.g., $p\gamma\to n\pi^+$ reactions, which decouples them instantaneously from the shell as long as their reconversion probability is low [64], which is the case for $\mathcal{D}>\mathcal{D}^*$ (cf. Sec. II A). This means that a low neutrino production efficiency corresponds to a low cosmic ray ejection efficiency for the standard scenario of shock acceleration, assuming magnetic confinement of all accelerated charged particles. This physical connection of both processes makes the hypothesis that gamma-ray bursts are the sources of the highest energy cosmic rays testable by neutrino VHE and UHE observations, both with respect to the flux and the maximum energy of the putative GRB correlated neutrino spectrum. It is also obvious from Fig. 2 that this joint scenario, i.e., $\hat{\mathcal{E}}_{p,20}\gtrsim 3$ and $\ell_\nu\gtrsim 0.04$, requires extreme values of the GRB parameters $\mathcal{D}$ and $\xi_{B\gamma}$.

V. CONCLUSIONS

We have presented a detailed investigation of the production processes of very energetic ($\gtrsim 10^{14}$ eV) photohadronic neutrinos in relativistically boosted astrophysical sources.

Using the constraints set by the source variability, and assuming that the acceleration process for protons is of the Fermi type, we derived limits on the maximum energy and the position of possible breaks in the neutrino spectrum. Comparing the effects of various cooling processes for both protons and secondary particles in the hadronic cascade leading to neutrino production (i.e., pions and muons), we find a general upper limit on the neutrino maximum energy, which does only depend on the Doppler factor of the emission region relative to the observer. Energetic constraints allow one to turn this into a general upper limit, which is only dependent on observational parameters of the transient, but not on any model dependent parameters. This is the major result of this paper. In some cases, and assuming that the energy in protons, magnetic field and photons are near equipartition, stricter limits can be imposed when considering both neutrino energy and expected flux. We apply this general result to two classes of proposed cosmic neutrino sources: hadronic models of Doppler beamed jets from active galactic nuclei (AGN), also called blazars, which are known to emit most of their energetic radiation in short, distinct flares, and gamma-ray bursts (GRBs).

For blazar flares, we confirm that under the most common assumptions the neutrino energy is limited to $\lesssim 10^{18}$ eV by Larmor radius (or adiabatic) constraints of the accelerated protons. For short ($\lesssim$1 h) flares, however, the maximum energy of neutrinos from muon decay may be additionally suppressed by muon synchrotron cooling. Assuming that the AGN is fueled by Eddington limited accretion on a supermassive black hole with $M_{\rm BH} \leqslant 10^{10} M_{\odot}$, we show that neutrinos from AGN flares cannot exceed energies of $\sim 10^{19}$ eV, independently of the time scale of the flare. For electron neutrinos, which result only from muon decay, we can show that fluxes of the magnitude usually assumed in the literature (i.e., similar to the x-ray luminosity of the source) can only be attained if the energy extends only up to about 10^{18} eV. Unless vacuum neutrino oscillations occur in nature, this has important implications for the neutrino event rates expected in the Pierre Auger Observatory, where electron neutrinos are proposed to be most easily detected because of the distinct properties of their induced air showers.

For GRBs we find that the synchrotron cooling of pions and muons limits the maximum neutrino energy over most of the allowed region of parameter space. We show that, although neutrinos from GRBs are in principle able to exceed 10^{19} eV, in particular for acceleration over long time scales in or near external shocks, this possibility would imply extremely low efficiencies and thus insignificant neutrino fluxes. If we require that neutrinos are also produced with fluxes similar to the γ-ray flux, and applying the usual energetic constraints for near-isotropic GRB sources, we find an upper limit on the neutrino energy of $\lesssim 10^{17}$ eV for muon neutrinos (from pion decay), and $\lesssim 10^{16}$ eV for electron neutrinos. This limit can only be increased to UHE ($>10^{17}$ eV) neutrino energies if strongly collimated outflows are assumed. We also show that the conditions for GRBs to accelerate protons up to the highest energies observed in cosmic ray air shower experiments ($\sim 3 \times 10^{20}$ eV) coincide with the conditions for efficient neutrino production, and expect a flat neutrino power spectrum extending up to a break energy in the range of 10^{16}–10^{18} eV. If neutrino production and cosmic ray ejection from GRB are connected processes, as implied by the standard assumption of magnetic confinement of shock accelerated particles in an expanding shell, this would make the hypothesis that gamma ray bursts are the sources of the observed ultrahigh energy cosmic ray spectrum testable with neutrino observatories.

As a corollary of our investigation of the relevance of secondary particle cooling to hadronic cascades in common models of astrophysical transients, we have also checked the effect of this process on other proposed, nontransient sources for cosmic neutrinos. In particular the predicted diffuse neutrino background from AGN cores, frequently used for event estimates in high energy neutrino detectors, was previously derived disregarding secondary particle cooling. Here we obtain for energies above 10^{15} eV a strongly reduced contribution and a lower cutoff in the electron neutrino component, and a reduction of about a factor 3 for the expected diffuse muon neutrino flux (see Appendix E).

In cosmic sources where the neutrino energy is limited by secondary particle cooling, which is clearly predicted for gamma-ray bursts and is possible in some blazar flares, the expected difference in the cutoff energy of electron and muon neutrinos could also serve as a laboratory to test the existence of neutrino vacuum oscillations in nature at very high energies—a detected change in the neutrino composition near the cutoff energy could rule out this possibility. Such a measurement would require a large detector sensitive in the range 10^{15}–10^{18} eV, capable of detecting both electron and muon neutrinos and able to distinguish between flavors.

ACKNOWLEDGMENTS

We wish to thank K. Mannheim and E. Zas for discussions. We also thank P. L. Biermann, T. Ensslin, and T. K. Gaisser for the careful reading of the manuscript, and helpful comments and suggestions. This work was supported in part by NASA grant NAG5-2857.

APPENDIX A: NOTATIONAL CONVENTIONS

Below we explain some general conventions we use throughout the paper. Table I lists some generally used symbols; it does not contain symbols which are used only in the section where they are defined.

(a) Units and normalized quantities. We use cgs units, except for particle energies which are given in standard multiples of electronvolts (eV, MeV, GeV, TeV), and particle interaction cross sections measured in microbarn (μb). In numerical calculations we use quantities normalized to common powers of their standard unit (stu), $X_n \equiv X/10^n$ stu (e.g., $L_{51} = L/10^{51}$ erg s^{-1}). Dimensionless quantities may be normalized in common powers as well. This convention is used consequently in Sec. IV, which means that numerical subscripts always denote normalization powers.

(b) Reference frames. Three reference frames are used in

TABLE I. Index of frequently used symbols.

symbol	meaning	definition/relations	introduced in
$m_\bullet$, $r_\bullet$, $\gamma_\bullet$	particle mass, classical radius, and Lorentz factor $[\bullet=p,\pi,\mu]$	$r_\bullet = e^2/m_\bullet c^2$	general
$\tau_\bullet$, $\tau_\bullet^{\rm RF}$	unstable particle lifetime $[\bullet=n,\pi,\mu]$	$\tau_\bullet = \gamma_\bullet \tau_\bullet^{\rm RF}$	Sect. II A
$\gamma_\star^{\rm pr}$, $\gamma_\star^{\rm dc}$	Lorentz factor of secondary particles at production, decay[b]	$\gamma_\mu^{\rm dc} \leq \gamma_\mu^{\rm pr} \approx \gamma_\pi^{\rm dc} \leq \gamma_\pi^{\rm pr} \approx \gamma_p$	Sect. II A
$N_{\rm ph}$, $N_{\rm ph,b}$, $\epsilon_{\rm b}$, a	total photon density, density and power law index above $\epsilon_{\rm b}$	$dN_{\rm ph} = \epsilon^{-a}\, d\epsilon$, $\epsilon > \epsilon_{\rm b}$	Sect. II A
$\epsilon_{\rm th}^{\rm RF}$	threshold photon energy in proton RF for π-production	Eq. (B2)	Sect. II A
$\gamma_{\rm b}$, $\tilde{\gamma}_{\rm b}$	characteristic Lorentz factor for power law approximation	$\gamma_{\rm b} = \epsilon_{\rm th}^{\rm RF}/2\epsilon_{\rm b}$, $\tilde{\gamma}_{\rm b} = \gamma_{\rm b}/\mathcal{D}$	Sect. II A
$t_{{\rm b},\pi}$, H_a	pion production cooling time for $\gamma_p = \gamma_{\rm b}$, effective inelasticity weighted cross section for power law photon spectrum	$t_{{\rm b},\pi} = [c\mathrm{H}_a N_{\rm ph,b}]^{-1}$, Eqs. (5), (16) (B2)	Sect. II A
B, $\omega_{B,\bullet}$	magnetic field, particle cyclotron frequency	$\omega_{B,\bullet} = eB/m_\bullet c$	Sect. II A
$t_{\bullet,{\rm syn}}$, $t_{\rm ad}$	particle synchrotron $[\bullet=\pi,\mu,p]$ and adiabatic cooling time[a]	Eq. (3), $t_{\rm ad} = 2\lvert B/\dot{B}\rvert$	Sect. II A
$t_{p\gamma}$, $t_{p,\pi}$, $t_{{\rm esc},n}$, $t_{p,{\rm BH}}$	total and specific photohadronic cooling times[a]	$t_{p\gamma}^{-1} = t_{p,\pi}^{-1} + t_{{\rm esc},n}^{-1} + t_{p,{\rm BH}}^{-1}$	Sect. II A
$\bar{t}_p$	total proton cooling time scale	$\bar{t}_p^{-1} = t_{\rm ad}^{-1} + t_{p,{\rm syn}}^{-1} + t_{p\gamma}^{-1}$	Sect. II A
$f_{p\gamma}$, $f_{\rm syn}$, $f_{\rm ad}$, $f_{\rm max}$	rate of proton cooling relative to pion production	Eq. (7)	Sect. II A
ζ_ν, $\zeta_{\nu,\star}$	efficiency for neutrino production, from specific decay[b]	Eq. (1)	Sect. II A
$\overline{u}_p$, b_p,	total *injected* proton energy density, bolometric correction factor	Eq. (8)	Sect. II B
$\hat{\gamma}_p$, s	maximum proton Lorentz factor, power law index	$d\dot{N}_p \propto \gamma_p^{-s}\, d\gamma_p$, $\gamma_p \lesssim \hat{\gamma}_p$	Sect. II B
$\bar{L}_\nu(E_\nu)$, $\hat{E}_\nu$, q	neutrino emission spectrum, cutoff energy, local spectral index	Eqs. (9)	Sect. II B
Γ, β_Γ, $\Theta_{\rm view}$, $\mathcal{D}$	bulk Lorentz factor, velocity in units of c, viewing angle and Doppler factor of the emission region in observers frame	$\beta_\Gamma = \sqrt{1-\Gamma^{-2}}$, $\mathcal{D} = [\Gamma(1-\beta_\Gamma \cos\Theta_{\rm view})]^{-1}$	Sect. III
$\mathcal{T}$, $L_{\rm b}$, $b_{\rm ph}$	observed duration of transient, luminosity at $\varepsilon = \varepsilon_{\rm b}$	$T = \mathcal{T}\mathcal{D}$, $\mathcal{L}_{\rm b} = L_{\rm b}\mathcal{D}^4$, Eq. (21)	Sect. III
$T_{\rm cr}$, $T_{\rm inj}$, $T_{\rm rad}$	transient crossing, proton injection and radiative time scale	Eq. (10)	Sect. III A 1
R, $R_\parallel$, $R_\perp$	linear size of transient emitter, $\parallel$ = in line of sight, $\perp$= projected	$R_\parallel = cT_{\rm cr}$	Sect. III
ρ_T, x_L	geometric correction factors	Eq. (11), (12)	Sect. III A 1
$r_{\rm L}$, $t_{\rm L}$	proton Larmor radius and time	$r_{\rm L} = E_p/eB$, $t_{\rm L} = 2\pi r_{\rm L}/c$	Sect. III B
$t_{\rm acc}$, $\theta_{\rm F}$	acceleration time scale, normalized to Larmor time	$t_{\rm acc} = \theta_{\rm F} t_{\rm L}$	Sect. III B
α, $\beta_{\rm ex}$,	magnetic field decay parameter, expansion velocity of transient	$B \propto R^{-\alpha}$, $\beta_{\rm ex} = \dot{R}/c$	Sect. III B 1
$\hat{\mathcal{E}}_{\nu,{\rm L}}$, $\rho_{\rm L}$	Larmor limit for neutrino energy, correction factor	Eq. (14), $\rho_{\rm L} \lesssim \min(\frac{1}{3}, \frac{1}{\pi\theta_{\rm F}\alpha\beta_{\rm ex}})$	Sect. III B 1
$\hat{\mathcal{E}}_{\nu,{\rm syn}(p)}$, $\hat{\mathcal{E}}_{\nu,p\gamma}$	neutrino cutoff energy limited by proton cooling[a]	Eqs. (15), (17)	Sect. III B
$\omega_\star$	characteristic frequency for secondary particle decay[b]	$\omega_\star = \frac{3}{2}\sqrt{c/\tau_\star^{\rm RF} r_\star}$	Sect. III C
$\tilde{\mathcal{E}}_{\nu,{\rm ad}(\star)}$, $\tilde{\mathcal{E}}_{\nu,{\rm syn}(\star)}$	critical neutrino energies for secondary particle cooling[a,b]	Eqs. (19), (20)	Sect. III C
$E_{\nu,\star}^{\rm RF}$	neutrino energy in decay frame[b]	$E_{\nu,\star} = \gamma_\star E_{\nu,\star}^{\rm RF}$	Sect. III C
$\Upsilon_{\mathcal{L}}$, $\Upsilon_{\mathcal{T}}$	dimensionless characteristic parameters of transient	Eqs. (18), (24)	Sect. III
u_B, u_e, $u_{\rm ph}$	magnetic, electron and photon energy density in emission region	$u_B = B^2/8\pi$, $u_e \sim u_{\rm ph}$	Sect. III D 1
$\xi_{B\gamma}$, $\bar{\xi}_{pB}$	energy equipartition parameters	Eq. (25), $\bar{\xi}_{pB} = \overline{u}_p/u_B$	Sect. III D 1
$\mathcal{D}^\star$, $B^\star$, $\hat{\gamma}_p^\star$	"star-point" parameters[c], all specific proton cooling times $=t_{\rm acc}$	Eqs. (23)	Sect. III D 1
$\hat{\hat{\mathcal{E}}}_{\nu,\bullet}(\mathcal{D})$, $\hat{B}_{{\rm syn}(\bullet)}$	neutrino energy limit and corresponding B for given $\mathcal{D}$ $[\bullet=p,\star]$[b]	Eqs. (27)–(31)	Sect. III D 2
$\hat{\hat{\ell}}_{\nu,\bullet}$	relative neutrino luminosity for $\hat{\mathcal{E}}_\nu = \hat{\hat{\mathcal{E}}}_{\nu,\bullet}$	Eqs. (34), (35)	Sect. III D 3
$\mathfrak{E}_{\rm T}$, $\xi_{B\gamma,{\rm max}}$	total energy budget of transient, corresponding maximum $\xi_{B\gamma}$	Eq. (36)	Sect. III D 3

[a]Cooling processes are: adiabatic losses (ad), synchrotron radiation (syn), photohadronic interactions ($p\gamma$), (charged) pion production ($\pi,\pi^\pm$), Bethe-Heitler $e^\pm$ pair production (BH), neutron escape (esc,n).

[b]The subscript "$\star$" denotes secondary particles in hadronic cascade here and throughout the paper $[\star=\pi^\pm,\mu]$

[c]The superscript "*" generally denotes quantities taken at the star-point of the parameter space, i.e., $\mathcal{D} = \mathcal{D}^\star$, $B = B^\star$, and $\gamma_p = \hat{\gamma}_p^\star$.

the paper: the observers frame, the comoving frame of the emission region (relativistic flow), and the rest frame of an interacting massive particle. Quantities are by default given in the comoving frame; quantities in the observers frame are denoted by calligraphic letters (e.g., $\mathcal{E}$, $\mathcal{T}$, $\mathcal{L}$, ε) of the same kind as corresponding quantities in the comoving frame (E, T, L, ϵ). Quantities in the particle rest frame are denoted with a superscript RF.

(c) Luminosity convention. Luminosities quoted in the paper always mean the isotropic radiated power at specific energy (frequency), e.g., $L = \epsilon^2(dN_{\rm ph}/d\epsilon)$ or $L_\nu = E_\nu^2(dN_\nu/dE_\nu)$. If we refer to bolometric luminosities, we do this by explicitly multiplying with a bolometric correction factor, e.g., $L_{\rm bol} \equiv b_{\rm ph} L_{\rm b}$ (see Table I). The energy output of a transient over its time scale T is denoted the *time integrated luminosity*, $\overline{L}$.

APPENDIX B: PHOTOHADRONIC INTERACTIONS

The major photohadronic interaction channels of protons are single pion production with and without isospin flip, $p\gamma \to n\pi^+$ and $p\gamma \to p\pi^0$, followed by several two-pion production channels, and multipion production which dominates at very high interaction energies. Secondary neutrons can contribute negative pions from $n\gamma \to p\pi^-$ reactions, which are otherwise only produced in two-pion and multi-pion

channels. The subsequent decay of the pions leads to neutrino production by

$$\pi^{\pm} \to \mu^{\pm} \nu_{\mu}(\overline{\nu_{\mu}}) \tag{B1a}$$

$$\mu^{\pm} \to e^{\pm} \overline{\nu}_{\mu} \nu_{e}(\nu_{\mu} \overline{\nu_{e}}). \tag{B1b}$$

The charge of the initial pion is only relevant for the $\nu{:}\overline{\nu}$ ratio; it plays a role for the electron neutrino component at energies $\mathcal{E}_{\nu} \approx 6 \times 10^{15}$ eV, where the detectability of $\overline{\nu_e}$ is enhanced due to the W^- resonance in interaction with atmospheric electrons. Otherwise, neither underwater or ice, nor air shower experiments can distinguish between neutrinos and antineutrinos, so that we can disregard the sign of the pion charge. The average energy of the neutrinos is determined by decay kinematics: it can be written as $\langle E_{\nu} \rangle = E^{\rm RF}_{\nu,\star} \gamma_{\star}$, where $E^{\rm RF}_{\nu,\star}$ is the energy of the neutrino in the rest frame of the decaying particle moving with Lorentz factor $\gamma_{\star}$. For pion decay, $E^{\rm RF}_{\nu,\pi} = 30$ MeV [35], while in the three particle decay of the muon $\langle E^{\rm RF}_{\nu,\mu} \rangle \approx \frac{1}{3} m_{\mu} c^2 = 35$ MeV; as an approximation, we may use $\langle E^{\rm RF}_{\nu,\star} \rangle \approx \frac{1}{4} m_{\pi} c^2$.

At low interaction energies, $\epsilon^{\rm RF} \sim 340$ MeV, the photohadronic cross section for both charged and neutral pion production is dominated by the $\Delta(1232)$ resonance, leading to single pion production with a $\pi^+{:}\pi^0$ ratio of 1:2 following isospin symmetry, and $E_{\pi} \approx 0.2 E_p$ from two-particle decay kinematics. These relations are often used as characteristic for pion production, and we call it the Δ-approximation [2,3]; it is quite accurate for π^0 production, in particular in steep photon spectra, and in thermal spectra with temperatures kT for proton Lorentz factors $\gamma_p \sim [340\ {\rm MeV}]/kT$, where higher resonances and other photohadronic interaction channels have little or no influence on the cross section. For charged pion production, however, other processes contribute significantly both above ($\epsilon^{\rm RF} \gtrsim 400$ MeV) and below ($\epsilon^{\rm RF}_{\rm th} < \epsilon^{\rm RF} \lesssim 250$ MeV) the dominance region of the $\Delta(1232)$ resonance, and thus enhance the contribution of charged pions relative to the Δ-approximation. These are in particular N^* resonances at energies above the $\Delta(1232)$, but cross section data also require a contribution from non-resonant pion production, which give an almost constant background of about 100 μb, extending from the immediate threshold [even before the $\Delta(1232)$ resonance becomes relevant] up to the highest energies [67,68]. In the neutrino sources considered in this paper, a proton spectrum extending up to a maximum energy $\hat{E}_p = m_p c^2 \hat{\gamma}_p$, interacts with an isotropic power law photon distribution, $dN_{\rm ph} \propto \epsilon^{-a} d\epsilon$, $a > 1$, extending from a break energy $\epsilon_{\rm b}$ to some cutoff at $\hat{\epsilon} \gg \epsilon_{\rm b}$, with a total number density $N_{\rm ph,b}$ of photons with $\epsilon > \epsilon_{\rm b}$. Below the break energy, we assume that the photon number spectrum is flatter than ϵ^{-1} everywhere. We can then define the inelasticity weighted effective cross section for pion production,

$$\mathrm{H}_a = 2 \frac{a-1}{a+1} \int_1^{\infty} dx x^{-a} \sum_i \left[\kappa_i \sigma_i \right]^{RF}_{\epsilon = x \epsilon^{\rm RF}_{\rm th}} \tag{B2}$$

for $a > 1$, where $\epsilon^{\rm RF}_{\rm th} \approx 145$ MeV is the threshold photon energy for pion production in the proton rest frame, σ_i is the cross section, and $\kappa_i = \langle \Delta E_p / E_p \rangle_i$ is the proton inelasticity of the reaction channel, evaluated at a photon energy $\epsilon^{\rm RF} = x \epsilon^{\rm RF}_{\rm th}$ in the proton RF (see [68] for details). Introducing the characteristic Lorentz factor $\gamma_{\rm b} = \epsilon^{\rm RF}_{\rm th} / 2 \epsilon_{\rm b}$ of the protons, which is necessary to boost background photons at the break energy above the reaction threshold for pion production, we can then write the cooling time of protons with $\gamma_p = \gamma_{\rm b}$ as $t_{{\rm b},\pi} = [c N_{\rm ph,b} \mathrm{H}_a]^{-1}$, where $N_{\rm ph,b}$ is the number density of photons with $\epsilon > \epsilon_{\rm b}$. As a function of γ_p the cooling time $t_{p,\pi}$ is then expressed by Eqs. (5), and we note that all the interaction physics, including the relative contributions of different resonances or other reaction channels, are absorbed in H_a and thus independent of the proton energy—this would not be the case in, e.g., thermal photon spectra, where our results are not applicable. As a numerical simplification, we also disregard the upper cutoff in the photon spectrum, which is justified if the spectrum for $\epsilon < \epsilon_{\rm b}$ is sufficiently steep—for spectra with $a < 2$, this approach is valid only in a limited range of Lorentz factors below $\gamma_{\rm b}$—and use $\mathrm{H}_a \approx \mathrm{H}_2/(a-1)$ for $1.5 < a \lesssim 3$, with $\mathrm{H}_2 \approx 22$ μb [68]. If $\gamma_p \gg \gamma_{\rm b}$, photohadronic interactions majorly happen at proton rest frame energies far above the threshold, where the cross section and efficiency is approximately constant; this justifies the approximation $t_{p,\pi} \approx [c N_{\rm ph} \mathrm{H}_2]^{-1}$, used throughout the paper.

If no other cooling processes apply, the average number of pions produced per proton can be found as $\langle N_{\pi}/N_p \rangle = \Pi_a / \mathrm{H}_a \approx 7$, for $1.5 < a \lesssim 3$, where Π_a is defined as in Eq. (B2) by replacing the proton inelasticity, κ_i, by the pion multiplicity of the reaction channel. The average energy carried by each pion is then, independent of γ_p, given by $\langle E_{\pi} \rangle / E_p \approx \frac{1}{7} \approx m_{\pi}/m_p$, i.e., the Lorentz factor can be treated as conserved in the interaction, $\gamma^{\rm pr}_{\pi} \approx \gamma_p$. Here, $\gamma^{\rm pr}_{\pi}$ is the pion Lorentz factor *at production*, which has to be distinguished from $\gamma^{\rm dc}_{\pi}$, the pion Lorentz factor *at decay*; for both pions and muons we consider the possibility that they lose energy during their lifetime, viz., $\gamma^{\rm dc}_{\star} \lesssim \gamma^{\rm pr}_{\star}$. Because of the small mass difference between pion and muon, we can also approximate $\gamma^{\rm pr}_{\mu} \approx \gamma^{\rm dc}_{\pi}$. Distinguishing between the charged pion and neutral pion multiplicity in the definition of Π_a yields the charged pion fraction, $\pi^{\pm}{:}\pi^0 \approx 2{:}1$, almost independent of the power law index a [68]. This result includes all reaction channels, and is in contrast to the often used ratio $\pi^{\pm}{:}\pi^0 = 1{:}2$, which is derived from the Δ-approximation. The discrepancy of a factor of 4 emphasizes the importance of charged pion production away from the Δ-resonance in power law target photon spectra, which is also relevant for the kinematics: it explains the difference of the usual assumption, $\langle E_{\pi} \rangle \approx \frac{1}{5} E_p$, (which is strictly valid for π^0 production, see above) and our result for charged pion production, $\langle E_{\pi} \rangle \approx \frac{1}{7} E_p$.

APPENDIX C: SENSITIVITY RANGE AND ENERGY DEPENDENCE OF NEUTRINO DETECTOR TECHNIQUES

The low detection probability for neutrinos above the TeV range requires large detector volumes, which can be achieved, e.g., by the extension of classical water Cherenkov

detectors to larger dimensions, such as the NESTOR or Lake Baikal (and the recently cancelled, pioneering DUMAND) experiments, and similar projects in the planning stage [2]. The same technique is also efficient in the deep antarctic ice, as shown impressively by the recent detection of the first neutrino events by the AMANDA experiment [69], and there is hope to extend this detector to an effective volume of 1 km^3 in the future [70]. A cost-efficient way to further increase the detector volumes could be the detection of radio pulses [71] or acoustic waves [72] from neutrinos in water or ice, which however are limited to very high energies to obtain a reasonable signal-to-noise ratio [2].

The neutrino event rate per logarithmic energy interval in a given detector, $\phi_{\nu,\mathrm{det}}$, can be written as the product of the neutrino *number* flux, $\mathcal{L}_\nu/\mathcal{E}_\nu$, times the detection probability, $P_{\nu,\mathrm{det}}$. For deep underwater/ice Cherenkov detectors, which are most efficient to detect muons from $\nu_\mu \to \mu$ conversions because of the large mean free path of muons in matter, the detection probability is essentially proportional to the ratio of the muon mean free path to the neutrino mean free path, yielding $P_{\nu,\mathrm{det}} \propto \mathcal{E}_\nu^{0.8}$ for $\mathcal{E}_\nu \gtrsim 10^{12}$ eV. At energies above $\sim 10^{14}$ eV the effective solid angle covered by the experiment is reduced by earth shadowing effects [73], so that this technique becomes ineffective for ultra high energies; it is also less sensitive to electron neutrinos, because the short range of the electron in matter reduces the effective volume. Radio Cherenkov detectors are proposed to work best in deep ice. The detection probability is usually expressed as the effective volume of the detector, increasing as $P_{\nu,\mathrm{det}} \propto \mathcal{E}_\nu^{1.5}$ for $\mathcal{E}_\nu \lesssim 10^{16}$ eV, and is roughly constant above 10^{16} eV [71]. The energy threshold for this technique is set by signal-to-noise constraints at $\sim 5 \times 10^{15}$ eV [2], thus in the relevant sensitivity range the detection probability can be treated as approximately constant. No clear predictions exist about the efficiency of the acoustic method yet, which is probably most interesting at ultrahigh energies.

Cosmic neutrinos may also cause air showers similar to cosmic rays, but deeper penetrating and thus distinguishable due to their large zenith angle [34]. At $\sim 10^{15}$ eV, such ''horizontal'' air showers are dominantly caused by atmospheric muons rather than cosmic neutrinos. Above 10^{17} eV, however, the atmospheric background becomes low, and the air scintillation technique used, e.g., in the HiRes Fly's Eye detector or the Telescope Array [74], largely improves the detectability of horizontal air showers, providing much larger detection volumes than underground detectors. Above $\sim 10^{19}$ eV, the planned Pierre Auger Observatory [75] is expected to achieve considerable event rates, using the same technique in conjunction with ground arrays for particle detection [12]. The main caveat of the technique is the large atmospheric background—horizontal air showers produced by muon neutrinos can be easily confused with air showers from atmospheric muons generated by the prompt decay of charmed particles [2,34]. Horizontal air showers produced by electron neutrinos have the unique property to be mixed hadronic and electromagnetic showers [34], which allows to determine distinctive triggering criteria for hybrid detectors like the Pierre Auger Observatory, reducing the background [12]. This makes electron neutrinos most interesting for UHE neutrino astronomy.

The detection probability for deeply penetrating horizontal air showers can be expressed as the product of the hadronic neutrino cross section, $\sigma_{\nu p}$, and the detector acceptance for an horizontal air shower. Models predict correspondingly that $\sigma_{\nu p} \propto \mathcal{E}_\nu^{0.5}$ for $\mathcal{E}_\nu \gtrsim 10^{15}$ eV [76]. The detector acceptance for the Pierre Auger Observatory has been calculated as $\propto \mathcal{E}_\nu^{0.3}$ for $\mathcal{E}_\nu \gtrsim 10^{17}$ eV, where horizontal air shower detection is expected to be more efficient than other techniques [12]. This gives rise to $P_{\nu,\mathrm{det}} \propto \mathcal{E}_\nu^{0.8}$, which is the same dependence as in the case in water or ice Cherenkov experiments. For other air shower experiments, the dependence of the shower acceptance on energy might be different, but a slow rise in the UHE regime seems to be a common feature.

The expressions for the energy dependence of the detection probability are highly approximate; exact results require expensive Monte Carlo simulations, considering the detailed properties of the experiment. However, we note that the neutrino event rate per logarithmic energy interval, evaluated for the most common detector techniques, follows closely the neutrino power spectrum, $\phi_{\nu,\mathrm{det}}/\mathcal{L}_\nu \sim \mathrm{const}$. An exception is only the range between 10^{15} eV and 10^{17} eV, where horizontal air shower observations are still dominated by the atmospheric background and underground experiments affected by earth shadowing.

APPENDIX D: TIME SCALES FOR FERMI ACCELERATION

The time scale for first order Fermi acceleration at parallel shock fronts (defined as having the flow direction parallel to the magnetic field lines, with perpendicular and oblique shocks defined accordingly) is given by [28]

$$t_{\mathrm{acc}} = \frac{\chi_\beta}{\chi_\beta - 1} \frac{r_{\mathrm{L}}}{c\beta_{\mathrm{sh}}^2} (y_- + \chi_\beta y_+), \tag{D1}$$

where β_{sh} is the velocity of the shock in the comoving frame of the unshocked fluid, and y_- and y_+ are the ratios of diffusion coefficients parallel to the magnetic field, $K_\parallel$, to the Bohm diffusion coefficient, viz., $y = 3K_\parallel / r_{\mathrm{L}} c \geq 1$, taken in the regions upstream and downstream from the shock, respectively. The velocity jump at the shock in its comoving frame, $\chi_\beta = \beta_- / \beta_+$, satisfies $\chi_\beta \leq 4$ in nonrelativistic shocks (for an ideal gas with specific heat index of $\frac{5}{3}$ [28]), and is $\chi_\beta = 3$ in the ultrarelativistic limit [77]. Assuming $y_+ \sim y_- \equiv y$, we find $\theta_{\mathrm{F}} \sim \beta_{\mathrm{sh}}^{-2} y$ since $\beta_{\mathrm{sh}} \equiv \beta_-$ by definition. For parallel shocks, there is no upper limit on the value of y, which can be interpreted as a measure for the strength of the turbulence in the magnetic field, $y \approx (B/\delta B)^2$. In perpendicular shocks, one can show that $\theta_{\mathrm{F}} \sim \beta_{\mathrm{sh}}^{-2} y/(1+y^2)$, and y is limited from kinetic theory and isotropy requirements by $y < \beta_{\mathrm{sh}}^{-1}$ [78]. In ultrarelativistic shocks, $\beta_{\mathrm{sh}} \approx 1$, Eq. (D1) is not strictly valid, but numerical simulations for both parallel and oblique relativistic shocks suggest $\theta_{\mathrm{F}} \sim 1$ [79], in corre-

spondence with the result of Eq. (D1) for $\beta_{\rm sh}=y=1$. The time scale for second order Fermi acceleration is given by [30]

$$t_{\rm acc}\approx\frac{3cr_{\rm L}}{v_{\rm A}^2}\left(\frac{\delta B}{B}\right)^{-2}. \tag{D2}$$

where $v_{\rm A}$ is the Alvén speed in the plasma. Introducing $y=(B/\delta B)^2$ as above, this yields $t_{\rm acc}\sim y\beta_{\rm A}^{-2}t_{\rm L}$, with $\beta_{\rm A}=v_{\rm A}/c$. The condition for efficient scattering of the particles is $\beta_{\rm A}^2\ll y$ [29], which directly translates to $\theta_{\rm F}\sim y\beta_{\rm A}^{-2}\gg 1$ for second order Fermi acceleration.

Hence, $t_{\rm acc}\sim t_{\rm L}=2\pi r_{\rm L}/c$, or $\theta_{\rm F}\sim 1$ gives a reasonable lower limit for the acceleration time scale of any kind of Fermi acceleration. It may be reached for acceleration in relativistic shock waves; in most cases, however, factors $\theta_{\rm F}\gtrsim 10$ would be more realistic. Throughout the paper, $\theta_{\rm F}$ is treated as constant, i.e., which assumes that the diffusion coefficient is proportional to the Bohm diffusion coefficient. This is not true in other turbulence spectra, e.g., Kolmogorov turbulence, where $\theta_{\rm F}\sim 1$ at the maximum energy implies $\theta_{\rm F}\gg 1$ at lower energies. While this can be important for the comparison of electron and proton acceleration time scales [80], it does not affect too much our results near the maximum proton energy.

APPENDIX E: VHE/UHE NEUTRINO EMISSION FROM AGN CORES

The first models which predicted considerable VHE-UHE neutrino fluxes from AGN assumed particle acceleration at shocks in the accretion flow onto the putative central black hole [6,7,37]. By assuming in these models that the power-law 2–10 keV x-ray emission observed from AGN is produced by π^0-decay from $p\gamma$ and pp interactions, and assuming that the observed diffuse x-ray background is entirely due to AGN, one can estimate the corresponding neutrino flux arising from pp and $p\gamma$ interactions. While the assumption of shocks in the accretion flow near the black hole is more speculative than in jets (unlike the shocks in extended jets, the inner portions of AGN have never been imaged with sufficient angular resolution to infer shocks), core shocks are still the most cited class of models used to estimate expected event rates in neutrino experiments. Thus, it useful to investigate such models for self-consistency in the face of the pion and muon cooling effects discussed in this paper, which were not considered in the published results (see also more recent papers, e.g., [8,10]).

In principle, we could incorporate these models into our general discussion, because the relevant sizes and time scales in AGN cores are also limited by variability. However, we will not write down here all the observational quantities, but use rather the physical parameters applied in the original papers. The only relevant quantity in the expression of the critical energy for pion and muon cooling [Eqs. (20)] is the value of the magnetic field, since AGN core models are obviously not Doppler boosted ($\mathcal{D}=1$). Assuming equipartition of the magnetic field and radiation energy densities, the magnetic field is generally taken as $B\sim[10^3\ {\rm G}]\mathcal{L}_{45}^{-1/2}$, where $\mathcal{L}_{45}$ is the UV luminosity of the AGN. (Note that the inverse dependence of the equipartition field on the luminosity arises from the fact that the luminosity scales with the distance of the shock from the black hole, and thus with the linear size of the acceleration region, as $\mathcal{L}\propto R$, leading to $u_{\rm ph}\propto\mathcal{L}^{-1}$.) Applying Eq. (20) this leads to $\tilde{\mathcal{E}}_{\nu,{\rm syn}(\mu)}\sim[10^{16}\ {\rm eV}]\mathcal{L}_{45}^{1/2}$, and $\tilde{\mathcal{E}}_{\nu,{\rm syn}(\pi)}\sim[10^{17}\ {\rm eV}]\mathcal{L}_{45}^{1/2}$. Disregarding pion and muon cooling, the models of Stecker *et al.* [6,10] predict a flat single-AGN neutrino power spectrum up to $[2\times10^{17}\ {\rm eV}]\mathcal{L}_{45}^{1/2}$ followed by an exponential cutoff; Protheroe and Szabo [37,8] find essentially the same result. The model of Sikora and Begelman [7] predicts a sharp cutoff at about 10^{15} eV due to their more conservative assumption for the acceleration time scale, $\theta_{\rm F}\sim 100\beta_{\rm sh}^{-2}$, rather than $\theta_{\rm F}\sim\beta_{\rm sh}^{-2}$ as assumed in the other models. The latter is the only model which is not modified by considering pion and muon cooling, while for the other models we see that the electron neutrino spectrum and 50% of the muon neutrino spectrum, arising from muon decay, steepen more than one order of magnitude lower in energy that previously assumed.

For the prediction of detector event rates, the integrated diffuse neutrino background contributed by all AGN needs to be determined. Taking simple step functions as approximations for both the steepening induced by muon cooling and the exponential cutoff induced by the maximum proton energy, and noting that the dependence of the maximum energy on the AGN x-ray luminosity remains the same, we can derive a relation which allows to transform the result obtained disregarding muon cooling into the result expected when this effect is considered. The ratio of the integrated neutrino number flux, $\mathcal{F}(\mathcal{E})$, to the unmodified single source spectrum, $f_0(\mathcal{E})$, for $\mathcal{E}$ between the cutoff energies of the least and most luminous AGN, can thus be written as

$$\mathcal{Q}(E)\equiv\frac{\mathcal{F}(\mathcal{E})}{f_0(\mathcal{E})}=\int_{\mathcal{L}_{\rm min}}^{\mathcal{L}_{\rm max}}\rho_{\rm AGN}(\mathcal{L})\Theta_{\rm H}(\hat{\mathcal{E}}\mathcal{L}_{45}^{1/2}-\mathcal{E})d\mathcal{L}, \tag{E1}$$

where $\rho_{\rm AGN}(\mathcal{L})$ is the AGN luminosity function, and $\Theta_{\rm H}(x)$ is the Heaviside step function, $\Theta_{\rm H}(x)=1$ for $x>0$ and $\Theta_{\rm H}(x)=0$ otherwise. Replacing $\hat{\mathcal{E}}\sim 2\times10^{17}$ eV, as originally assumed, by $\hat{\mathcal{E}}'=10^{16}$ eV as obtained from muon cooling, obviously leads to the relation $\mathcal{Q}'(\mathcal{E})=\mathcal{Q}(\mathcal{E}\hat{\mathcal{E}}/\hat{\mathcal{E}}')\approx 0.05\mathcal{Q}(\mathcal{E})$, since $\mathcal{Q}\propto\mathcal{E}^{-1}$ [6,37]. Since $\mathcal{Q}'/\mathcal{Q}=\mathcal{F}'/\mathcal{F}$, the diffuse flux of electron neutrinos (as well as muon neutrinos from muon decay) is reduced to about 5% of the value previously obtained, independent of the luminosity function used. Additionally, the exponential cutoff of the diffuse background, corresponding to the cutoff of the most luminous quasars, sets in already below 10^{17} eV rather than at 10^{18} eV. Similarly, the diffuse muon neutrino flux from pion decay is reduced to about 50% of the original value, so that the total VHE muon neutrino flux drops by about a factor of 3 and cuts off at 10^{18} eV.

Clearly, a more detailed calculation is required to obtain reliable flux rates under consideration of detailed spectral modification induced by pion and muon cooling, but our ap-

proximate results already show that the effect is important. In particular, we expect no considerable contribution from AGN cores to the electron neutrino spectrum in the energy range interesting for horizontal air shower measurements. No change of the predicted fluxes is expected in the energy range relevant for deep underwater or ice Cherenkov detectors, like Lake Baikal or AMANDA. In the interesting intermediate range, in particular relevant for the event prediction for proposed radio Cherenkov detectors, we obtain a moderately lower flux of muon neutrinos, and a severely reduced contribution of electron neutrinos. Since the model prediction are upper limits (constrained by the diffuse x-ray background), the drop in the rates cannot be balanced by adjusting astrophysical parameters.

[1] Y. Totsuka, Rep. Prog. Phys. **55**, 377 (1992).

[2] T. Gaisser, F. Halzen, and T. Stanev, Phys. Rep. **258**, 173 (1995).

[3] F. Stecker, Astrophys. Space Sci. **20**, 47 (1973); Astrophys. J. **228**, 919 (1979).

[4] E. Zas, in *Very High Energy Phenomena in the Universe*, Proceedings of the 32nd Rencontres de Moriond, Les Arcs, 1997, edited by Y. Giraud-Héraud and J. Trân Thanh Vân (Editions Frontières, Paris, 1997), pp. 37–42, astro-ph/9704016.

[5] G. Sigl, S. Lee, D. Schramm, and P. Coppi, Phys. Lett. B **392**, 129 (1997).

[6] F. Stecker, C. Done, M. Salamon, and P. Sommers, Phys. Rev. Lett. **66**, 2697 (1991); **69**, 2738(E) (1992).

[7] M. Sikora and M. Begelman, in *High Energy Neutrino Astrophysics*, edited by V. J. Stenger, J. G. Learned, S. Pakvasa, and X. Tata (World Scientific, Singapore, 1992), pp. 114–129.

[8] A. P. Szabo and R. J. Protheroe, Astropart. Phys. **2**, 375 (1994).

[9] K. Mannheim, Astropart. Phys. **3**, 295 (1995).

[10] F. W. Stecker and M. H. Salamon, Space Sci. Rev. **75**, 341 (1996).

[11] F. Halzen and E. Zas, Astrophys. J. **488**, 669 (1997).

[12] G. Parente and E. Zas, in *Neutrino Telescopes*, Proceedings of the 7th International Symposium, Venice, 1996, edited by M. Baldo-Ceolin (Dept. Physics, Univ. of Padua, 1996), p. 345, astro-ph/9606091; K. S. Capelle, J. W. Cronin, G. Parente, and E. Zas, Astropart. Phys. **8**, 329 (1998).

[13] B. Paczyński and G. Xu, Astrophys. J. **427**, 708 (1994).

[14] E. Waxman and J. Bahcall, Phys. Rev. Lett. **78**, 2292 (1997).

[15] J. E. McErny *et al.*, in ''25th International Cosmic Ray Conference, Durban, 1997,'' OG4.3.4, astro-ph/9706125; R. J. Protheroe *et al.*, *ibid.*, astro-ph/9710118.

[16] K. Mannheim, Astron. Astrophys. **269**, 67 (1993); Space Sci. Rev. **75**, 331 (1996).

[17] M. Sikora, G. Madejski, and M. Begelman, in *Relativistic Jets in AGN*, Proceedings of the Cracow Conference, 1997, edited by M. Ostrowski, M. Sikora, G. Madejski, and M. Begelman (Astronomical Observatory, Jagiellonian University, 1997), astro-ph/9708261.

[18] P. Mészáros and M. J. Rees, Astrophys. J. Lett. **482**, L29 (1997).

[19] P. L. Biermann, J. Phys. G **23**, 1 (1997), and references therein.

[20] G. R. Blumenthal and R. J. Gould, Rev. Mod. Phys. **42**, 237 (1970).

[21] K. Mannheim, W. M. Krülls, and P. L. Biermann, Astron. Astrophys. **251**, 723 (1991).

[22] J. Jackson, *Classical Electrodynamics*, 2nd ed. (Wiley, New York, 1975), pp. 588–593.

[23] M. J. Rees, Mon. Not. R. Astron. Soc. **184**, 61P (1978).

[24] M. J. Rees and P. Mészáros, Astrophys. J. Lett. **430**, L93 (1994).

[25] R. D. Blandford and C. F. McKee, Phys. Fluids **19**, 1130 (1976).

[26] R. Sari and T. Piran, Astrophys. J. Lett. **455**, L143 (1995).

[27] E. Fermi, Phys. Rev. **75**, 1169 (1949); Astrophys. J. **119**, 1 (1954).

[28] L. O'C. Drury, Rep. Prog. Phys. **46**, 973 (1983).

[29] D. B. Melrose, *Plasma Astrophysics: Nonthermal Processes in Diffuse Magnetized Plasmas* (Gordon and Breach, New York, 1980), Vol. II.

[30] R. M. Kulsrud, in *Particle Acceleration Mechanisms in Astrophysics*, edited by J. Arons, C. Max, and C. McKee, AIP Conf. Proc. No. 56 (American Institute of Physics, New York, 1979), pp. 13–26.

[31] W. M. Krülls, Astron. Astrophys. **260**, 49 (1992).

[32] M. Sikora, M. C. Begelman, and M. J. Rees, Astrophys. J. **421**, 153 (1994).

[33] B. Rudak and P. Mészáros, Astrophys. J. **383**, 269 (1991).

[34] E. Zas, F. Halzen, and R. Vázquez, Astropart. Phys. **1**, 297 (1993).

[35] Particle Data Group, R. M. Barnett *et al.*, Phys. Rev. D **54**, 1 (1996).

[36] G. M. Webb, L. O'C. Drury, and P. Biermann, Astron. Astrophys. **137**, 185 (1984); W. Krülls and A. Achterberg, *ibid.* **286**, 314 (1994).

[37] R. J. Protheroe and A. P. Szabo, Phys. Rev. Lett. **69**, 2885 (1992).

[38] K. Mannheim, T. Stanev, and P. L. Biermann, Astron. Astrophys. **260**, L1 (1992).

[39] M. Catanese *et al.*, Astrophys. J. Lett. **487**, L143 (1997).

[40] E. Pian *et al.*, Astrophys. J. Lett. **497**, L17 (1998).

[41] F. Aharonian *et al.*, Astron. Astrophys. **327**, L5 (1997).

[42] A. Mastichiadis and J. G. Kirk, Astron. Astrophys. **320**, 19 (1997).

[43] J. H. Buckley, Science **279**, 676 (1998); K. Mannheim, *ibid.* **279**, 684 (1998).

[44] E. J. Guerra and R. A. Daly, Astrophys. J. **491**, 483 (1997).

[45] C. M. Urry and P. Padovani, Publ. Astron. Soc. Pac. **107**, 803 (1995).

[46] K. Mannheim, in *Gamma Ray Emitting AGN*, Proceedings of the Heidelberg Workshop, 1996, edited by J. G. Kirk, M. Camenzind, C. von Montigny, and S. Wagner (MPI Kernphysik, Heidelberg, 1996), pp. 57–60, astro-ph/9612066.

[47] L. M. J. Brown *et al.*, Astrophys. J. **340**, 129 (1989).
[48] P. Grandi *et al.*, Adv. Space Res. **15**, 23 (1995).
[49] J. A. Gaidos *et al.*, Nature (London) **383**, 319 (1996).
[50] J. H. Buckley *et al.*, Astrophys. J. Lett. **472**, L9 (1996).
[51] G. Lamer and S. Wagner, Astron. Astrophys. **331**, L13 (1998).
[52] T. Takahashi *et al.*, Astrophys. J. Lett. **470**, L89 (1996).
[53] A. Celotti, A. C. Fabian, and M. J. Rees, Mon. Not. R. Astron. Soc. **293**, 239 (1998).
[54] R. D. Blandford and M. J. Rees, Mon. Not. R. Astron. Soc. **169**, 395 (1974); R. D. Blandford and A. Königl, Astrophys. J. **232**, 34 (1979).
[55] C. Thompson, Mon. Not. R. Astron. Soc. **270**, 480 (1994).
[56] M. Schubnell, in *Proceedings of the 4th Compton Symposium, Williamsburg, 1997*, edited by C. D. Dermer, M. S. Strickman, and J. D. Kurfess, AIP Conf. Proc. No. 410 (American Institute of Physics, New York, 1997), astro-ph/9707047.
[57] G. J. Fishman and C. A. Meegan, Annu. Rev. Astron. Astrophys. **33**, 415 (1995).
[58] P. Mészáros, in *Gamma-Ray Bursts*, Proceedings of the 4th Huntsville Symposium, 1997, edited by C. A. Meegan, R. Preece, and T. Koshut, AIP Conf. Proc. No. 428 (American Institute of Physics, New York, 1998), pp. 647–656, astro-ph/9711354.
[59] C. Kouveliotou, Science **277**, 1257 (1997), and references therein; S. Kulkarni *et al.*, Nature (London) **393**, 35 (1998).
[60] P. Mészáros, in 17th Texas Symposium on Relativistic Astrophysics and Cosmology, edited by H. Böhringer, G. E. Morfill, and J. E. Trümper [Ann. (N.Y.) Acad. Sci. **759**, 440 (1995)].
[61] E. Waxman, Phys. Rev. Lett. **75**, 386 (1995).
[62] M. Vietri, Astrophys. J. **453**, 883 (1995).
[63] P. Mészáros and M. J. Rees, Astrophys. J. **405**, 278 (1993).
[64] J. P. Rachen and P. Mészáros, in *Gamma-Ray Bursts*, Proceedings of the 4th Huntsville Symposium, 1997, edited by C. A. Meegan, R. Preece, and T. Koshut, AIP Conf. Proc. No. 248 (American Institute of Physics, New York, 1998), pp. 776–780.
[65] M. Vietri, Phys. Rev. Lett. **80**, 3690 (1998).
[66] E. Waxman and J. Bahcall, Phys. Rev. D (to be published), hep-ph/9807282.
[67] J. M. Laget, Phys. Rep. **69**, 1 (1981).
[68] J. P. Rachen, Ph.D. thesis, MPIfR, Universität Bonn, Germany, 1996, http://www.astro.psu.edu/users/jorg/PhD.
[69] F. Halzen, in *WIN 97*, Proceedings of the XVI International Workshop on Weak Interaction and Neutrinos, Capri, 1997, edited by G. Fiorillo, V. Palladin, and P. Strolin [Nucl. Phys. B (Proc. Suppl.) **66**, 155 (1998)], astro-ph/9707289.
[70] F. Halzen, Comments Nucl. Part. Phys. **22**, 155 (1997).
[71] G. Frichter, J. Ralston, and D. McKay, Phys. Rev. D **53**, 1684 (1994).
[72] A. Butkevitch *et al.*, in *Particles and Cosmology*, edited by E. Alexeev, V. A. Metveev, Kh. S. Nirov, and V. Rubakov (World Scientific, Singapore, 1996), pp. 306–315.
[73] A. Nicolaidis and A. Taramopoulos, Phys. Lett. B **386**, 211 (1996).
[74] T. Abu-Zayyad *et al.*, in *Proceedings of the 25th International Cosmic Ray Conference*, Durban, South Africa, 1997, edited by M. S. Potgieter *et al.* (World Scientific, Singapore, 1998), OG 10.6.1; S. Aiso *et al.*, *ibid.*, OG 10.6.15.
[75] M. Boratav, in *TAUP 95*, Proceedings of the 4th International Workshop on Theoretical Aspects of Underground Physics, Toledo, Spain, 1995, edited by A. Morales, J. Morales, and J. A. Villar [Nucl. Phys. B (Proc. Suppl.) **48**, 488 (1996)], pp. 488–490.
[76] R. Gandhi, C. Quigg, M. H. Reno, and I. Sarcevic, Astropart. Phys. **5**, 81 (1996).
[77] J. G. Kirk and P. Schneider, Astrophys. J. **315**, 425 (1987).
[78] J. Jokipii, Astrophys. J. **313**, 842 (1987).
[79] D. C. Ellison, F. C. Jones, and S. P. Reynolds, Astrophys. J. **360**, 702 (1990); J. Bednarz and M. Ostrowski, Mon. Not. R. Astron. Soc. **283**, 447 (1996).
[80] P. L. Biermann and P. A. Strittmatter, Astrophys. J. **322**, 643 (1987).